



UNIVERSITY OF LEEDS

This is a repository copy of *A Raman spectroscopy based optical fibre system for detecting carbonation profile of cementitious materials*.

White Rose Research Online URL for this paper:  
<http://eprints.whiterose.ac.uk/123626/>

Version: Accepted Version

---

**Article:**

Yue, Y, Wang, JJ, Basheer, PAM [orcid.org/0000-0002-0835-8029](https://orcid.org/0000-0002-0835-8029) et al. (2 more authors) (2018) A Raman spectroscopy based optical fibre system for detecting carbonation profile of cementitious materials. *Sensors and Actuators B: Chemical*, 257. pp. 635-649. ISSN 0925-4005

<https://doi.org/10.1016/j.snb.2017.10.160>

---

© 2017 Elsevier B.V. This manuscript version is made available under the CC-BY-NC-ND 4.0 license <http://creativecommons.org/licenses/by-nc-nd/4.0/>

**Reuse**

This article is distributed under the terms of the Creative Commons Attribution-NonCommercial-NoDerivs (CC BY-NC-ND) licence. This licence only allows you to download this work and share it with others as long as you credit the authors, but you can't change the article in any way or use it commercially. More information and the full terms of the licence here: <https://creativecommons.org/licenses/>

**Takedown**

If you consider content in White Rose Research Online to be in breach of UK law, please notify us by emailing [eprints@whiterose.ac.uk](mailto:eprints@whiterose.ac.uk) including the URL of the record and the reason for the withdrawal request.



[eprints@whiterose.ac.uk](mailto:eprints@whiterose.ac.uk)  
<https://eprints.whiterose.ac.uk/>

## Accepted Manuscript

Title: A Raman spectroscopy based optical fibre system for detecting carbonation profile of cementitious materials

Authors: Yanfei Yue, Jing Jing Wang, P.A. Muhammed Basheer, John J. Boland, Yun Bai



PII: S0925-4005(17)32074-9  
DOI: <https://doi.org/10.1016/j.snb.2017.10.160>  
Reference: SNB 23464

To appear in: *Sensors and Actuators B*

Received date: 3-3-2017  
Revised date: 25-10-2017  
Accepted date: 26-10-2017

Please cite this article as: Yanfei Yue, Jing Jing Wang, P.A.Muhammed Basheer, John J.Boland, Yun Bai, A Raman spectroscopy based optical fibre system for detecting carbonation profile of cementitious materials, *Sensors and Actuators B: Chemical* <https://doi.org/10.1016/j.snb.2017.10.160>

This is a PDF file of an unedited manuscript that has been accepted for publication. As a service to our customers we are providing this early version of the manuscript. The manuscript will undergo copyediting, typesetting, and review of the resulting proof before it is published in its final form. Please note that during the production process errors may be discovered which could affect the content, and all legal disclaimers that apply to the journal pertain.

# **A Raman spectroscopy based optical fibre system for detecting carbonation profile of cementitious materials**

Yanfei Yue<sup>ab</sup>, Jing Jing Wang<sup>c††</sup>, P. A. Muhammed Basheer<sup>d</sup>, John J. Boland<sup>c</sup> and Yun Bai<sup>b†</sup>

<sup>a</sup> College of Materials Science and Engineering, Chongqing University, 174 Shazheng Street, Shapingba, Chongqing, China 400044

<sup>b</sup> Department of Civil, Environmental and Geomatic Engineering, University College London, Gower Street, London, WC1E 6BT, UK

<sup>c</sup> CRANN and AMBER Research Centres, Trinity College Dublin, Dublin 2, Dublin, Ireland

<sup>d</sup> School of Civil Engineering, University of Leeds, Woodhouse Lane, Leeds, LS2 9JT, UK

† Dr Yun Bai. Email: [yun.bai@ucl.ac.uk](mailto:yun.bai@ucl.ac.uk). Tel: +44(0)20 76792386.

†† Dr Jing Jing Wang. Email: [JJWANG@tcd.ie](mailto:JJWANG@tcd.ie). Tel: 00353 18964633.

## **Highlights**

- A bespoke Raman spectroscopy based optical fibre sensing platform capable of detecting the internal chemistry of cementitious materials has been successfully established.**
- The calcium carbonate and its profile have been successfully detected by this optical fibre Raman system.**
- The study demonstrates a good potential for developing a Raman spectroscopy based embeddable optical fibre sensor network for monitoring the chemistry and the durability of concrete structure.**

## **Abstract**

Sensors demonstrate huge potential in civil engineering for monitoring the health condition and performance of concrete structures. Amongst various chemical deterioration mechanisms causing

inadequate durability of concrete structures, carbonation is one of the most severe mechanisms. It occurs from the chemical reactions between intruded  $\text{CO}_2$  and calcium-bearing phases, hence is accompanied by the formation of calcium carbonate ( $\text{CaCO}_3$ ) and the decrease of the alkalinity of concrete pore solution, causing corrosion of rebar in concrete. Thus, detecting carbonation process, especially, determining the carbonation profile (i.e. the content of carbonation products formed against the depth into concrete structure), is of great importance to the diagnosis of the health condition of concrete structures and the prediction of service life. Unfortunately, existing sensors for health monitoring systems suffer from various limitations. Optical fibre Raman technology offers a unique opportunity for developing a novel chemical sensor system capable of monitoring the service-condition of concrete in situ. In the current work, a bespoke ‘coaxial’ optical fibre sensing platform based on Raman spectroscopy was successfully established with a 514.5 nm laser. All the optics were tailored for efficiently exciting and receiving signals from cementitious materials, and their diameters were restricted within 0.5 inch in order to explore the feasibility of developing an embeddable miniature sensor system in the future. This sensing system was then employed to detect the carbonation mechanism of a plain Portland cement (PC) paste. The calcium carbonate polymorphs as well as the carbonation profile in the PC paste was successfully recognised and established with the results being verified favourably by bench-mounted Raman, X-ray Diffraction (XRD) and Thermogravimetry (TG) analyses. Our results demonstrate a good potential for developing a novel Raman spectroscopy based optical fibre sensor system for monitoring the health condition and the performance concrete structures in future.

**Keywords:** Calcium carbonate, Carbonation, Concrete, Optical fiber sensor, Raman spectroscopy, Sensing platform

---

## 1. Introduction

Recent decades have witnessed some interest in developing sensor devices for monitoring the physical properties (e.g., strain) of concrete structures [1, 2]. However, as concrete are exposed to different environment (such as  $\text{CO}_2$  and  $\text{SO}_4^{2-}$ ), it would trigger chemical deteriorations due to the interaction between concrete and exposure environment. Monitoring the changes of internal chemistry of concrete is, hence, more important as this can provide insight into the cause and evolution of the deterioration mechanisms as well as the prediction of health-condition and performance of concrete structures [3]. Amongst the various deterioration mechanisms initiating the durability issues of concrete structures, carbonation is a severe deterioration mechanism causing the inadequate durability of reinforced concrete [3, 4]. It is mainly a chemical process occurred when the calcium-bearing phases, such as calcium hydroxide (CH), calcium silicate hydrate (CSH) and various calcium aluminate or ferro-aluminate hydrates, in cement matrix are attacked by carbon dioxide ( $\text{CO}_2$ ) penetrated into concrete through the pore network [5-8]. The dominant reaction is the one between calcium hydroxide [ $\text{Ca}(\text{OH})_2$ ] and  $\text{CO}_3^{2-}$  (i.e., the carbon dioxide dissolved in concrete pore solution) to form calcium carbonate ( $\text{CaCO}_3$ ). This process lowers the pH of concrete pore solution from about 13 to 8.3, in the case of complete carbonation [9, 10]. At this pH level, the passive film formed on the surface of steel bar could be destroyed, leading to the initiation of the corrosion of rebar in the presence of oxygen and moisture [3, 10]. Additionally, CSH gel could also be attacked, leading to a reduction of Ca/Si ratio from around

1.75 to a lower value of 0.67 at the early stage of carbonation, followed by a subsequent transformation into calcium carbonate and amorphous silica gel by further carbonation [5, 11]. Although this reaction, unlike the carbonation of calcium hydroxide, does not affect the alkalinity of pore solution, it favours the decomposition of CSH and, hence, reduces the stability and strength-carrying capacity of cement matrix. Obviously, carbonation changes the cement chemistry of the internal concrete remarkably, with the most prominent aspect of forming calcium carbonate [12]. The calcium carbonate phases precipitated within the cementitious materials could exist in different polymorphs, such as, calcite (well-crystallised phase) and vaterite/aragonite (poor-crystallised phases) [12, 13]. Generally, the content of calcium carbonate decreases with increasing distance from the exposed surface of concrete, which is caused by the decreased degree of carbonation due to the reduced penetration of CO<sub>2</sub> into the interior part of concrete [14-16]. However, with increased exposure to CO<sub>2</sub>-bearing environment, the depth of carbonation increases with time. As it is the cover concrete which provides the protection to the embedded rebar, differentiating the type of calcium carbonate polymorphs formed within the cover concrete, but more importantly, determining the carbonation profile in terms of the content of calcium carbonate phases over the depth of cover concrete and also over time, is of great importance for predicting the service life of concrete structures [17]. Moreover, it can provide valuable information for the diagnosis of health condition of concrete structures so that timely actions could be taken before any severe damages could be initiated.

Numerous studies have been reported in the literature on the investigation of concrete carbonation [12, 13, 15, 18-21]. The phenolphthalein spray test, by spraying phenolphthalein indicator solution onto a freshly exposed concrete surface and visually inspect the sprayed

section, is probably the most well-known method to assess the carbonation depth of concrete [19, 22]. As phenolphthalein turns purple at about  $\text{pH} > 8.3$  and remains colourless when  $\text{pH} \leq 8.3$ , the deep-purple colour on the uncarbonated area and the clear area of the carbonated region on the surface of concrete can be immediately differentiated [23, 24]. This test is convenient, quick and cheap. However, although this test can give reproducible results to indicate the fully carbonated region, it cannot differentiate the boundary between uncarbonated and partially carbonated concrete or the boundary between partially carbonated and fully carbonated concrete where  $\text{pH}$  may have only dropped to around 10-12 [25]. It is, therefore, generally accepted that the phenolphthalein method may underestimate the carbonation front [26, 27]. To address this issue, researchers have attempted to employ other techniques to study the carbonation in cementitious materials, including Thermogravimetry (TG)/Derivative Thermogravimetry (DTG) [12, 15, 20], X-ray Diffraction (XRD) [12, 13], Fourier transform infrared spectroscopy (FTIR) [18, 19, 26], Gammadensimetry [15, 21] and Mercury Intrusion Porosimetry (MIP) [28, 29]. However, most of these methods are laboratory based and sample need to be taken from the structures, even though it only causes little damage to the structure. To obtain non-destructive, continuous and real-time information about the condition of concrete structure, there is an increasing interest and rapid advancement in developing sensor system for monitoring the chemical environment of concrete, such as carbonation/ $\text{pH}$  profile, especially within the cover zone [30-32]. Amongst the sensors capable of monitoring the properties of cover concrete, electrical sensors (ES) have attracted tremendous attentions and the most widely used is electrical resistance based sensor, such as covercrete electrode array (CEA) [32, 33]. CEA measures the conductance, or resistance, across the electrode pairs mounted at discrete depths in cover-zone and, hence, give valuable insight into the spatially distributed moisture and ionic

movement within the cover concrete. However, the limitation associated with the ES mainly lies in its inadequacy in differentiating, uniquely, each individual deterioration mechanism, such as carbonation, as the electrical properties of concrete can also be affected by other factors such as moisture change, ions ingress and ongoing hydration. Due to this reason, fibre optic sensors (FOS) have attracted tremendous attentions in recent years for its merits of inert nature, immunity to electromagnetic interference, lightweight/miniature and multiplexing into multi-sensing [34-36]. More importantly, FOS can overcome the drawback of ES by encapsulating the fibre tip with specific chemical dyes so that each individual deterioration mechanism can be uniquely differentiated [30, 36-38]. For example, fibre optic pH sensor has demonstrated its potential in following the pH variation in concrete due to carbonation and this could provide some timely information on the progress of carbonation within the cover concrete [30, 37]. However, FOS suffers from its irreversibility and instability of the chemical dyes in the inherently aggressive environment of the pore solution of concrete [36, 39]. On the other hand, attempts have also been made by the researchers to monitor the condition of rebars in concrete directly, such as the Anode-Ladder system developed by P. Schießl and M. Raupach, which can be used to monitor the galvanic current between the pairs of anode-cathode and hence, can provide invaluable information on the corrosion rate of the rebars [40, 41]. Although this system also can provide an early warning of the possible corrosion, it cannot provide the information needed to understand the chemical reactions incurred in cover concrete. Hence, there is still a need to develop a more reliable and robust sensor system which can be used to effectively monitor the health condition and the performance, in particular the possible chemical reaction involved, of concrete structures subjected to different deterioration mechanisms, such as carbonation.



Since 1970's, Raman spectroscopy has attracted increasing attentions worldwide in analysing various phases in cement and concrete area due to its fingerprint characterisation capacity based on the measurement of the vibrational spectra of analytes [42-49]. In particular, Raman spectroscopy has demonstrated its unique capability to identify different calcium carbonate polymorphs, such as calcite, vaterite and aragonite [50-58]. In recent years, by combining the qualitative/quantitative characterisation capability of Raman spectroscopy and the light transmission of optical fibres, optical fibre Raman technology has shown its potential as a next-generation sensing system. Above all, the rapid developments of instrumentation, such as the portable Raman spectrometer, the long-distance and low-loss optical fibre and some sophisticated functional optics, offer a huge potential for a monitoring system based on optical fibre Raman spectroscopy technology and, indeed, researchers have already been exploring its applications in the areas such as biomedical diagnosis [59, 60], chemistry process monitoring [61, 62] and operations in detrimental environment [63, 64]. However, surprisingly, this technique is not currently being attempted in the area of cement and concrete. During the past few years, the authors have been taking the initiative to explore the potential of developing an optical fibre Raman sensing system to characterise the deterioration mechanisms of cementitious materials, with an ultimate target to develop a Raman spectroscopy based embeddable optical fibre sensor network capable of monitoring and evaluating the health condition and the performance of concrete structures on site. Our preliminary work have confirmed the feasibility of characterising the deterioration products formed during the sulphate and carbonation attacks in hardened cement paste by a tailored fibre-optic excitation pathway (e.g., fibre excitation path + objective collection) [65, 66]. However, to fully verify the feasibility of developing a future fibre optic

Raman based sensor system, both the excitation path and the signal collection path should be made from optical fibre. Hence, the current work expands our previous studies by:

- i) developing a bespoke ‘coaxial’ optical fibre sensing platform based on Raman spectroscopy, with both the laser-excitation and signal-collection sub-paths consisting of optical fibres (i.e., fibre excitation + fibre collection);
- ii) establishing the carbonation profile using the newly developed Raman based optical fibre sensing system. The carbonation profile was then verified by bench-mounted Raman spectroscopy (i.e. Raman spectroscopy without fibre), X-ray Diffraction (XRD) and Thermogravimetry (TG) analyses.

## **2. Material and methods**

### **2.1 Sample preparation**

#### **2.1.1 Materials**

Portland cement (PC) used in this study was CEM I (in accordance with BS EN 197-1:2011 [67]) supplied by QUINN Group (Derrylin, UK) and its chemical composition is given in Table 1. The pure calcium carbonate (Assay > 98%), employed as a reference in this study, was purchased from the Fisher Scientific (Loughborough, UK). An acrylic paint (Sikaguard 680-s), provided by Sika Lt. UK, was used to coat the curved face and the trowel-finished face of the hardened cement cylinders before the accelerated carbonation.

### 2.1.2 Manufacture of PC paste

The cement paste was manufactured with a water-to-cement ratio (W/C) of 0.5 using a Hobart planetary mixer. Immediately after mixing, the bottom-half of the cylindrical moulds ( $\text{Ø}50 \times 80$  mm PVC moulds) were filled with the paste and were compacted using a vibrating table until air bubbles stopped appearing on the paste surface. Then, the top-half of the moulds were filled and compacted again by the vibrating table until air bubbles stopped appearing on the paste surface. After the second layer was compacted, a steel scraper was used to clear up and smooth the top of the specimen surface. Immediately after casting, the moulds were sealed with lids, and stored in a curing room at a constant temperature of  $20(\pm 1)$  °C and Relative Humidity (RH) of  $55(\pm 5)$  % for 24 hours. The specimens were then removed from the moulds and each specimen was wrapped with a water-saturated hessian before being sealed in an air-tight plastic bag. The specimens were again stored in the same curing room for another 55 days.

### 2.1.3 Conditioning and carbonation of PC paste

After the initial curing for 56 days, the paste cylinders were dried in an oven at  $40(\pm 1)$  °C for 14 days. Following this, the specimens were wrapped individually with polythene sheets and the joints were sealed with parcel-tape. The sealed specimens were again placed in the  $40(\pm 1)$  °C oven for another two weeks to allow the redistribution of the moisture inside the cylinders in order to establish a uniform moisture distribution within the specimens before the carbonation process. The trials indicated that a drying and humidity redistribution regime like this is sufficient for achieving an internal RH of about  $60(\pm 5)$  %. After the humidity redistribution, the

specimens were taken out of the oven and allowed to cool down to room temperature of  $20(\pm 1)$  °C for one day. Following the cooling process, the paste cylinders were unsealed from the polythene sheets and the curved face and the trowel-finished face were then coated by three layers of acrylic paint (Sikaguard 680-s), leaving only the face cast against the mould exposed to CO<sub>2</sub> attack. The painting was dried under  $20(\pm 1)$  °C for five days, after which the specimens were ready to be exposed to carbonation. The carbonation chamber (LEEC, UK) was set to maintain a constant temperature of  $20(\pm 1)$  °C, a carbon dioxide (CO<sub>2</sub>) concentration of  $5(\pm 0.5)$  % and  $60(\pm 5)$  % RH. The coated specimens were exposed to this carbonation environmental for six weeks before being removed from the chamber.

After carbonation, powder samples were collected at five discrete depths (i.e. 0-2 mm, 5-7 mm, 10-12 mm, 15-17 mm and 20-22 mm) of the specimens, by means of a digital drill (accuracy of 0.1mm) with a bit of 8 mm diameter and 4 mm deep slant edge. The powder generated between the intervals at 2~5 mm, 7~10 mm, 12-15 mm and 17-20 mm were carefully removed by a vacuum cleaner. This was to avoid any contamination to the powder samples collected at the targeted depths which were used to establish the carbonation profile. The powder samples collected at each targeted depth interval were then passed through a 63 µm sieve. Particles smaller than 63 µm were then transferred to air-tight plastic bags and stored in the vacuum desiccators before being analysed by Raman spectroscopy (without/with optical fibre), XRD and TG.

## **2.2 Bench-mounted Raman spectroscopy**

A Renishaw micro-Raman spectroscope equipped with a Charged Coupled Device (CCD) detector was applied under controlled temperature of 20 °C. A 514.5nm single-line (Argon ions) laser was employed as the excitation source. The laser beam was focused into a laser spot about  $4.95 \mu\text{m}^2$  through a LEICA (Germany) N Plan objective with 10X magnification, and then interrogated the sample. Measured power at the sampling level was around 3.2 mW. The Raman shift was calibrated before each experiment using the sharp peak of  $\text{TiO}_2$  (anatase) powder. Raman spectra were recorded with exposure time of 10s and accumulations of 10 to improve the signal-to-noise ratio (SNR). In this study, the bench-mounted Raman spectroscopy analysis was used to verify the Raman spectra obtained from the optical fibre Raman system as detailed below.

## **2.3 Raman Data Process**

The Raman data were analysed with the employment of OriginPro 8.6 (Origin, USA) and by following the procedures as detailed below:

### **2.3.1 Data collection**

Due to the heterogeneous nature of cementitious materials, five different sampling points were analysed at each depth from the carbonated powder samples. Each Raman spectrum was first normalised by the power density, and then processed as per to the following steps to retrieve the Raman peak features.

### 2.3.2 Background subtraction

During the initial trials, it was realised that background could always occur which imposed strong disturbance to the identification of the intrinsically weak Raman peaks. During the data process, to eliminate this troublesome background, baseline correction (i.e., background subtraction) using OriginPro 8.6 was employed first to subtract the background. After subtracting the background, the Raman peaks those were obscured previously by the fluorescence could be clearly observed.

### 2.3.3 Peaks fitting

After subtracting the background, the Raman peaks of the powder samples were fitted with Lorentz function, to retrieve the four Raman peak features, i.e., peak wavenumber, peak height, peak area and peak full-width-at-half-maximum (FWHM). The peak wavenumber contains the fingerprint information for differentiating the analytes [42], e.g., calcium carbonate polymorphs formed during the carbonation, whilst the peak height and the peak area are related to their quantity [68]. In this study, the peak height and peak area of  $\nu_1$  CO<sub>3</sub>, after being normalised by power density, were compared in terms of their applicability as the indicator of calcium carbonate content.

### 2.3.4 Calculation of signal-to-noise ratio (SNR)

The signal-to-noise ratio (SNR) is one of the most important parameters of the Raman spectra, which can indicate the quality of the spectra. In the current study, the SNR was employed to quantitatively compare the spectra obtained from the optical fibre Raman system and bench-mounted Raman spectrometer. The signal intensity and noise level of the five normalised Raman spectra obtained at each depth were averaged first. The SNR values were then calculated according to the method specified in ASTM E579-04 [69], as follows:

$$SNR = \frac{\text{Signal level}}{\text{Noise (RMS)level}} \quad (1)$$

Where, the signal level is the peak intensity after subtracting the background;

the noise level is obtained by root mean square (RMS) method, which is the standard deviation of the intensity values of a selected Raman shift region on the spectrum after subtracting the background.

## 2.4 X-ray Diffraction (XRD)

X-ray diffraction (XRD) was adopted in this study as a supplementary technique to qualitatively verify the mineralogical compositions of the carbonated powder samples. The tests were carried out using a PANalytical X'Pert PRO MPD diffractometer with an X-ray source of copper (Cu). A step size of  $0.016^\circ 2\theta$  were used to examine the samples in the range of  $5^\circ$  to  $70^\circ 2\theta$ . The X-ray tube voltage and current were fixed at 40 kV and 40 mA, respectively.

## 2.5 Thermogravimetry (TG)

TG analysis was conducted to quantify the calcium carbonate formed in the carbonated PC paste powder. The TG analysis was performed with a NETZSCH STA 449C instrument under an inert N<sub>2</sub> environment (flow rate of 1 ml/min). The samples were placed in an alumina (Al<sub>2</sub>O<sub>3</sub>) crucible and heated from room temperature to 1000 °C at a heating rate of 20 °C/min. The derivative thermogravimetric curve (DTG) were recorded simultaneously.

The quantification of calcium carbonate was considered by following its decomposition as follows:



First, the beginning and end temperature points related to the decomposition of calcium carbonate formed at each sampling depth was determined by considering TG and DTG curves.

Following this, the percentage of this phase was calculated by Eq. (3) below [70]:

$$W_i(\%) = \frac{(m_1 - m_2) * M_i}{M_r} \quad (3)$$

Where, W<sub>i</sub> is the percentage of the CaCO<sub>3</sub>, %.

m<sub>1</sub> is the mass of the powder sample at the mass-loss beginning point, %.

m<sub>2</sub> is the mass of the powder sample at the mass-loss end point, %.

M<sub>i</sub> is the molar-mass of CaCO<sub>3</sub> (100.09), g/mol.

M<sub>r</sub> is the molar-mass of CO<sub>2</sub> (44.01), g/mol.

### 3. Results and discussion

#### 3.1 Establishment of optical fibre sensing platform based on Raman spectroscopy (optical fibre Raman system)



### 3.1.1 Establishment of optical fibre platform

In this study, after a careful comparison of various possible optical configurations, the ‘coaxial’ backscattering with  $180^\circ$  sampling geometry was finally determined as the most suitable set up for this fibre optic sensing platform for characterising the solid calcium carbonate distributed within cementitious matrix [71-78]. This configuration employs a dichroic filter so as to combine the laser transmission axis with the collection axis immediately before sampling objective to form a ‘coaxial’ pathway, which can, hence, work under backscattering geometry to analyse most materials with any states, especially solids. What’s more, ‘coaxial’ configuration offers various advantages such as better signal reproducibility, capacity of pre-alignment and flexibility with the focus objective. More importantly, it demonstrates a unique potential to be converted into a compact configuration suitable for future sensor system [71, 72, 76]. A schematic diagram of the Raman spectroscopy based ‘coaxial’ optical fibre sensing system established in this study is presented in Fig.1

The key features of this configuration, elaborated under the excitation path and the collection path respectively below, include:

- i) **Excitation path.** An optical fibre (1#) was employed to deliver the laser beam (hereafter referred to as “excitation fibre”). The output laser was coupled into the excitation fibre (1#) by means of a laser adapter. After passing through the excitation fibre, the divergent laser beam was collimated first by a collimator (1#). A bandpass filter with centred wavelength at 514.5 nm was then installed in order to eliminate the plasma lines and also

the silica ( $\text{SiO}_2$ ) Raman scattering generated from the fibre core [73, 77, 79]. Following this, the laser beam was reflected by a mirror into a dichroic filter and finally launched into a microscope objective (1#). After focusing by this objective, the laser spot was used to interrogate the sample.

- ii) **Collection path.** The Raman scattered lines were first collected and paralleled by the same objective (1#) as in the excitation path and these then passed through the dichroic filter, by which the frequency shifted Raman signal from the sample was transmitted while the Rayleigh-scattered laser radiation was rejected [71, 72, 76]. After passing through the dichroic filter, the signal was launched into the collection fibre (2#) through another collimator (2#) and finally coupled into the same bench-mounted Raman spectrometer (as described below) by a second objective (2#) for subsequent signal process.

Building upon this design, the various tailored optics, such as fibres, filters and mirror, which were parameter-specified for efficiently exiting and collecting the Raman signals from cementitious materials, were constructed into the optical fibre platform after tremendous alignment work. The optical fibre platform established [80] in the laboratory is shown in Fig. 2. It should be noted that the diameters of all the optics were restricted within 0.5 inch in order to verify the concept of using mini-optics in terms of laser excitation and Raman-signal collection, with the final target to develop this optical fibre platform into a miniature sensor system with appropriate package regime. Through the above configuration, the concept of transmitting laser through optical fibre and then collecting Raman signal through optical fibre was tested in this

study, which can then be used to verify the potential of an optical fibre Raman system for monitoring the carbonation of concrete structures in the future.

### 3.1.2 Calibration

Prior to calibrating the optical fibre Raman system, bench-mounted Raman spectrometer as the core instrument was calibrated first. In the current study,  $\text{TiO}_2$  (anatase) powder was selected as the calibration standard due to its strong Raman signals, and similar powder status with samples. Its sharp peaks between  $300\text{ cm}^{-1}$  and  $800\text{ cm}^{-1}$  were used as the reference bands in the calibration. The Raman spectra of  $\text{TiO}_2$  under the bench-mounted Raman spectroscopy and the ‘coaxial’ optical fibre Raman system are reported in Fig. 3. Table 2 summarises the Raman bands of the  $\text{TiO}_2$  identified under both bench-mounted Raman and optical fibre Raman systems.

As can be seen from Fig. 3, the Raman spectra of  $\text{TiO}_2$  under these two Raman systems showed very similar features, i.e., both spectra were dominated by three sharp peaks at the Raman shift region of  $350 - 750\text{ cm}^{-1}$ . Furthermore, from Table 2, it is evident that the three reference peaks

were almost identical under these two Raman systems, with the peak wavenumbers corroborate well the results reported in the literature [81]. The above results suggest that both the ‘coaxial’ optical fibre Raman system and the bench-mounted Raman system have been well calibrated with high comparability with each other and are ready to use.

### 3.1.3 Laser power detection

After the establishment of this Raman spectroscopy based ‘coaxial’ optical fibre platform, the laser power through this optical pathway was monitored prior to the experiment to track the laser power passing through the fibre, so that the laser transmission/coupling efficiency in bench-mounted Raman and optical fibre Raman systems could be compared. Table 3 reports the laser status at different locations of the two Raman systems. As can be seen from Table 3, the coupling efficiency between the laser output and the excitation fibre was very high, i.e., 90%, indicating a good coupling at the laser-fibre interface. Furthermore, it should be noted that the power and also the power density under these two Raman systems were different. Although the same laser generator was used in both Raman systems, the excitation power of the optical fibre Raman system (10.4 mW) was much higher than that of the bench-mounted Raman spectroscopy (3.2 mW), which could be attributed to the less transmission and high reflection loss of the bench-mounted Raman pathway. However, the power density of the fibre Raman system was still lower than that of the bench-mounted Raman system, i.e.,  $0.38 \text{ mW}/\mu\text{m}^2$  vs  $0.65 \text{ mW}/\mu\text{m}^2$ , which is caused by the big difference existing in the size of the laser spots (i.e.,  $27.33 \mu\text{m}^2$  of optical fibre Raman and  $4.95 \mu\text{m}^2$  of bench-mounted Raman) between these two Raman systems.

### 3.2 Characterisation of pure calcium carbonate

A pure calcium carbonate ( $\text{CaCO}_3$ , main phase is calcite) with assay level above 98% was used as the reference material, and was characterised by optical fibre Raman system, with the results obtained being verified by bench-mounted Raman analysis. This test was used as a quick method to confirm the capability of the optical fibre Raman system established for recognising calcite, the main product formed in carbonation. At the same time, the Raman spectra collected were also used as bench-marks for the subsequent optical fibre Raman system analysis of the carbonation products formed in the cement samples subjected to accelerated carbonation attack.

The spectrum of  $\text{CaCO}_3$  recorded by optical fibre Raman system is presented in Fig. 4(a). As can be seen from the original spectrum in Fig. 4(a), sloping background emerged at  $300\text{ cm}^{-1}$  and onwards can be observed, which imposes disturbance to the identification of the genuine Raman peaks such as the band at  $1436\text{ cm}^{-1}$  ( $\nu_3$  asymmetric stretching vibration of  $\text{CO}_3$ ). This unwanted background may be caused by various factors, such as the intrinsic Raman pathway, incorporation of fibre and optics as well as the contribution from the fluorescence due to impurities in the raw materials [73, 78, 79]. Hence, the background of the spectrum was subtracted using OriginPro 8.6. The resultant spectrum is shown in Fig. 4(b). It can be seen that after subtracting the background, all the Raman bands became clearer. This much improved visibility of Raman peaks in Fig. 4(b) after background subtraction would suggest that background subtraction is a useful technique for processing the Raman spectra, especially for those obtained from the optical fibre Raman system. Therefore, in the following sections, only the Raman spectra after subtracting the background will be reported (unless otherwise stated).

As can be seen from Fig. 4(b), the optical Raman spectrum of the pure calcium carbonate was dominated by a pronounced and intense peak located at  $1084\text{ cm}^{-1}$ , which is the characteristic of the  $\nu_1$  symmetric stretching band of the  $\text{CO}_3$  groups in calcite. At the same time, three minor bands were also identified at  $280\text{ cm}^{-1}$ ,  $711\text{ cm}^{-1}$  and  $1434\text{ cm}^{-1}$ , which can be attributed to the Ca-O lattice vibration (LV), the in-plane bending ( $\nu_4$ ) and the asymmetric stretching ( $\nu_3$ ) vibration in calcite, respectively. All these bands and related assignments are summarised in Table 4.

Figs. 5 (a) and (b) present the original spectrum and background subtracted spectrum of  $\text{CaCO}_3$  collected under bench-mounted Raman spectroscopy, respectively. Evidently, the Raman signal of calcite has been well retrieved by bench-mounted Raman system, i.e. a well-defined peak at  $1086\text{ cm}^{-1}$  ( $\nu_1\text{ CO}_3$ ), a sharp peak at  $280\text{ cm}^{-1}$  (LV) and two bands located at  $712\text{ cm}^{-1}$  ( $\nu_4\text{ CO}_3$ ) and  $1436\text{ cm}^{-1}$  ( $\nu_3\text{ CO}_3$ ), respectively. Related bands are also summarised in Table 4. By comparing Figs. 4(b) and 5(b), it is apparent that, as shown in Table 4, the fingerprint bands identified from optical fibre Raman system are in good agreement with those from bench-mounted Raman spectroscopy, indicating that the optical fibre Raman system has achieved identical function as that of bench-mounted Raman spectroscopy for characterising calcite.

### 3.3 Characterisation of the PC paste

Following the success in characterising the pure calcite with optical fibre Raman system, the calcium carbonate polymorphs formed at the different depths of the carbonated PC paste cylinders were analysed in order to identify the potential of optical fibre Raman system for establishing carbonation profile in PC-based cementitious matrices. The experiments and, accordingly, the relevant discussion, were organised in the following three steps:

- i) Identification of the qualitative working capacity of the optical fibre Raman system for characterising the calcium carbonate polymorphs formed in the carbonated PC paste. This part of the study aimed at demonstrating whether the ‘coaxial’ optical fibre Raman system can differentiate the calcium carbonate formed under different degrees of carbonation within a bulk PC paste – in this case, the calcium carbonate polymorphs formed at five different depths (hence different degrees of carbonation would be expected) of the carbonated PC paste cylinders were investigated. Again, the Raman peak shift was used as the indicator of the different vibrations existing in different calcium carbonate phases. The bench-mounted Raman spectroscopy and XRD analyses were also carried out to provide additional qualitative information to verify the optical fibre Raman results.
- ii) Identification of the quantitative working capacity of the optical fibre Raman system for characterising the content of calcium carbonate formed at five different depths of the carbonated PC paste. To quantify the content of calcium carbonate, the first step was to decide which Raman parameter should be used to establish the quantitative information. Two parameters of Raman spectra of calcium carbonate, namely, peak height and peak area which are generally considered to be able to provide quantitative information of the analytes [75], were selected as the quantitative indicators and compared with the quantitative information obtained from TG analysis. Through this comparison, the most

suitable parameter was identified and used as the quantity indicator in the subsequent investigation.

- iii) Establishment of the carbonation profile of PC paste using the above determined appropriate content indicator, viz. peak height, of calcium carbonate obtained from optical fibre Raman system. The carbonation profile established from optical fibre Raman system was then compared with the carbonation profiles obtained from bench-mounted Raman spectroscopy and TG analysis in order to verify the reliability of optical fibre Raman system.

### **3.3.1 Identification of the qualitative working capacity**

#### **3.3.1.1 Optical fibre Raman analysis**

Fig. 6 depicts the Raman spectra of the carbonated PC paste powder samples at five different depths recorded by the ‘coaxial’ optical fibre Raman system. As can be seen from Fig. 6, in the optical fibre Raman spectra obtained from the samples collected at the depths of 0-2 mm, 5-7 mm and 10-12 mm, a sharp peak emerged at about  $1085\text{ cm}^{-1}$  which is the  $\nu_1\text{ CO}_3$  symmetric stretching band. This result indicates that calcite and/or aragonite were formed [50-58] at these near surface zones due to the ingress of  $\text{CO}_2$ . The intensity of this  $\nu_1\text{ CO}_3$  band decreased with the increase of the depth which is expected from a typical carbonation profile, i.e. the content of calcium carbonate formed should decrease with the increase of the carbonation depth. This peak ( $\nu_1\text{ CO}_3$ ) was absent from the spectra collected from the two deeper layers, i.e., 15-17 mm and 20-22 mm, suggesting that the carbonation front did not reach these depths. A peak emerged at



about  $1123\text{ cm}^{-1}$  could be assigned to the huntite phase according to the literature [82]. Besides, the minor vibration bands such as the  $\text{CO}_3$  in-plane bending ( $\nu_4$ ) mode were not recognised under the optical fibre Raman system, which raises the possible sensitivity issue of the optical fibre Raman system. Nonetheless, as the  $\nu_1$   $\text{CO}_3$  band is the most primary internal vibration band, this result confirms the adequate qualitative working capacity of the optical fibre sensing platform for characterising the calcium carbonate polymorphs in carbonated PC paste. However, it should be noted that, compared to the spectra obtained from the bench-mounted Raman spectroscopy (shown in Fig. 7), the peak intensity of the optical fibre Raman spectra was lower but its noise level was much higher (this issue will be discussed below).

### 3.3.1.2 Bench-mounted Raman analysis

The spectra of the carbonated PC paste powder collected from the bench-mounted Raman spectroscopy are shown in Fig. 7. Similarly, in bench-mounted Raman spectra, a well-defined peak was visible at about  $1085\text{ cm}^{-1}$  ( $\nu_1$   $\text{CO}_3$ ) and dominated the spectra of the powder samples collected at the depths of 0-2 mm, 5-7 mm and 10-12 mm. The growth of this band towards the surface of the PC paste was clear, indicating a higher degree of carbonation at the near surface zones. This result corroborates the results obtained from the optical fibre Raman system, indicating good comparability between the ‘coaxial’ optical fibre Raman system and the bench-mounted Raman spectroscopy. Apart from the intense  $\nu_1$   $\text{CO}_3$  peak, the  $\text{CO}_3$  in-plane bending ( $\nu_4$ ) mode was also identified at the depths of 0-2 mm and 5-7 mm, as evidenced by the band recognised at about  $707\text{ cm}^{-1}$ . The hump at about  $996\text{ cm}^{-1}$  ( $\nu_1$   $\text{SO}_4$ ) could be from the gypsum in the raw cement [45, 83].

### 3.3.1.3 Verification of the formation of calcium carbonate polymorphs by XRD analysis

Fig. 8 shows the XRD patterns of the carbonated PC paste powder collected at the five different depths, which were used to qualitatively verify the calcium carbonate polymorphs formed. As highlighted before, the primary reaction during the carbonation process is the one between CO<sub>2</sub> and portlandite [CH, Ca(OH)<sub>2</sub>], leading to the formation of different calcium carbonate polymorphs. From the XRD patterns in Fig.8, the calcium carbonate polymorphs, i.e., calcite and/or vaterite/aragonite, were identified from the powder samples collected at the first three depths (i.e., 0-2 mm, 5-7 mm and 10-12 mm), as manifested by their typical XRD peaks, i.e.  $2\theta = 29.4^\circ$ ,  $36.0^\circ$  and  $39.4^\circ$  for calcite,  $2\theta = 24.8^\circ$ ,  $27.1^\circ$  and  $32.8^\circ$  for vaterite and  $2\theta = 26.3^\circ$ ,  $41.2^\circ$  and  $45.8^\circ$  for aragonite, respectively. Moreover, in general, the intensity of these peaks decreased with the increase of the depth. No calcium carbonate was observed in the samples collected at the depths of 15-17 mm and 20-22 mm. All these observations accord well with the findings from optical fibre Raman system, as well as bench-mounted Raman spectroscopy. On the other hand, portlandite was also recognised in all the five sampling depths in the carbonated PC paste cylinders. As expected, it showed inverse trend to the calcium carbonate, i.e., with the increase of the depth, the peak of the CH increased.

### 3.3.2 Identification of the quantitative working capacity

To identify the quantitative working capacity of the optical fibre Raman system, TG analysis was firstly employed to quantify the calcium carbonate formed in the carbonated PC paste samples. Two Raman peak features, namely, peak height and peak area, were then selected as potential

indicators to quantify the calcium carbonate. By comparing with the TG results, the peak height, in particular, the peak height of the most intense peak of the carbonates, i.e.  $\nu_1$   $\text{CO}_3$  symmetric stretching band, was identified as the most suitable indicator to quantify the carbonates formed in hardened PC paste samples. Details of these results and the related discussions are presented below.

### 3.3.2.1 TG analysis

TG/DTG has been widely used to quantify different cement hydration and deterioration products [12, 15, 20, 77]. Fig. 9 and Fig. 10 show the TG and DTG curves of the carbonated PC paste powder from five different depths, respectively. In Fig. 9, the sharp decrease of the TG curves indicates the mass-loss of powder upon heating, which is associated with the decomposition of certain phases. Correspondingly, DTG diagrams exhibited well-defined endothermic peaks. The features of the two most important phases associated with carbonation, i.e., calcium carbonate and calcium hydroxide (CH) can be observed and summarised as follows:

- i) Calcium carbonate. As shown in Fig. 10, there were three apparent troughs at about 520 °C ~ 840 °C for the samples collected at the depths of 0-2mm, 5-7mm and 10-12 mm. Correspondingly, the dramatic mass-loss were observed at the same temperature range in the TG curves (Fig. 9), i.e., 500 °C ~ 840 °C. This temperature range corresponds to the decomposition of calcium carbonate, probably including three modes, i.e., 780 °C ~ 990 °C for calcite, 680 °C ~ 780 °C for vaterite and aragonite and 550 °C ~ 680 °C for amorphous phases. This result is in consistent with the XRD analysis results as shown in

Fig. 8, in which the three calcium carbonate polymorphs were identified in the first three depths of the carbonated PC paste cylinders.

- ii) Calcium hydroxide (Portlandite). The decomposition of portlandite occurred at about 450 °C ~ 520 °C as evidenced by the sharp endothermic peaks observed at this temperature range (Fig. 10).

Hence, the calcium carbonate and calcium hydroxide (CH) in the carbonated PC paste samples were quantified with TG/DTG [12, 15, 20, 70]. Their contents (%) over the depth of the carbonated PC cylinder samples were calculated using Eq. (3) and are plotted in Fig. 11.

From Fig. 11, it can be seen that the content of calcium carbonate decreased with increasing depth which is expected from a typical carbonation profile. Moreover, a considerable amount of  $\text{CaCO}_3$  was identified at the first three depths of the carbonated PC paste cylinders, i.e., 25.2%, 21.4% and 8.7% for the depths of 0-2 mm, 5-7 mm and 10-12 mm, respectively. From the depth of 15-17mm downwards, the amount of  $\text{CaCO}_3$  decreased sharply to about 5%, possibly owing to the substantial decrease of the ingress of  $\text{CO}_2$  at these depths. In contrast, considerable amount (> 13%) of CH existed in the carbonated PC paste cylinders from the depth of 10-12 mm downwards and only few amount of CH was identified at the first two depths (0-2 mm and 5-7 mm), which showed an exactly opposite trend to the calcium carbonate profile, i.e., the amount of calcium carbonate decreased with the depth, while the amount of CH increased with the depth. This phenomenon can be well explained by the fact that, the formation of calcium carbonate from carbonation reaction is always accompanied by the consumption (and hence the reduction)

of calcium hydroxide. It is, thus, reasonable to expect more CH in the deeper depth, whereas less CH and more calcium carbonate at the shallow depth of the carbonated PC samples.

### **3.3.2.2 Selection of the most suitable Raman peak feature as the indicator for quantifying the calcium carbonate content**

As aforementioned, the Lorentz function (after baseline correction) was employed to fit the Raman peaks of calcium carbonate. Under the Lorentz function, the following four features of a particular peak can be obtained, i.e., wavenumber, height, area and FWHM (full width at half maximum), which can be illustrated as follows:

- i) Wavenumber ( $X_c$ ,  $\text{cm}^{-1}$ ) – the Raman shift of certain ionic groups;
- ii) Height (H) – the intensity of the peak above the corrected baseline;
- iii) Area (A) – the integrated area of the peak above the corrected baseline;
- iv) FWHM (W,  $\text{cm}^{-1}$ ) – the full-width-at-half-maximum of the peak.

Obviously, these four Raman peak features indicate distinct information about the analytes. The wavenumber of the Raman peak is the fingerprint information to distinguish the materials – as each ionic group has its own unique wavenumber under laser excitation [42]. The FWHM is considered to be related to the degree of crystallisation of the analytes [84]. The other two features, i.e., peak height and peak area, are both related to the quantity of the analytes [68]. However, in the literature, there is no information available to confirm which of these two features is more suitable to quantify the calcium carbonate formed in cementitious materials. Thus, there is a need to compare these two peak features in order to identify which one is more suitable to quantify the carbonation products formed. As  $\nu_1$   $\text{CO}_3$  symmetric stretching band is the

most intense peak of the carbonates, it was, hence, selected as the reference band in the following study.

#### a) Optical fibre Raman analysis

Table 5 presents the peak wavenumber, peak height and peak area of the  $\nu_1$   $\text{CO}_3$  band of the optical fibre Raman spectra of the PC paste powder collected at five different depths. The calcium carbonate contents obtained from the TG analysis are also reported. As can be seen, the calcium carbonate was identified in the first three depths of the carbonated PC paste cylinders by optical fibre Raman system, which corroborates well the XRD analysis shown in Fig. 8. However, the fibre Raman system did not pick up the trace amount of  $\text{CaCO}_3$  existed at the depth of 15-17 mm and 20-22 mm, although these have been retrieved by TG analysis. This result indicates that, although the 'coaxial' fibre Raman system can show a general trend of the calcium carbonate formed during the carbonation, unlike TG analysis, it is still not sensitive enough to differentiate the calcium carbonate at the trace levels. Nonetheless, both the peak height and peak area decreased over the depths within the first three layers, indicating their potential as an index to quantify the calcium carbonate formed. To identify which of these two Raman peak features is the most suitable indicator, the calcium carbonate content obtained from the TG analysis was plotted against the peak height and peak area respectively in Fig. 12 and Fig. 13. As shown in Figs. 12 and 13, there were good correlations between TG and both peak height and peak area obtained under optical fibre Raman system. However, a better  $R^2$  was identified between the peak height and TG (0.99). Hence, the peak height is considered a more suitable peak feature for optical fibre Raman system.

## b) Bench-mounted Raman analysis

Table 6 summarises the wavenumber, height and area of the  $\nu_1$  CO<sub>3</sub> peak of the spectra of the carbonated PC paste samples obtained from bench-mounted Raman system. Similar to the optical fibre Raman system, the bench-mounted Raman system did not identify the trace level calcium carbonate formed at the depths of 15-17 mm and 20-22mm. Therefore, future study still needs to be carried out to improve the sensitivity of Raman spectroscopic systems for characterising trace amounts of analytes (e.g., calcium carbonate) which is, in particular, important for the possible future monitoring system in concrete. Similar to the data analysis carried out for the optical fibre Raman platform, the calcium carbonate content obtained from the TG analysis was plotted against the peak height and peak area in Fig. 14 and Fig. 15, respectively. As shown in Figs. 14 and 15, both the peak height and peak area identified under the bench-mounted Raman analysis demonstrated good correlations with the calcium carbonate content measured by TG analysis. However, the  $R^2$  value against TG from peak height (0.97) was relatively higher than that from peak area (0.95). This finding is the same as that obtained from the optical fibre Raman analysis, indicating again that the peak height is the most suitable peak feature to quantify the calcium carbonate formed in the carbonated cement pastes.

Therefore, based on the characterisation and correlation analysis from both Raman systems, the peak height is considered as the most suitable indicator to quantify the content of calcium carbonate formed during the carbonation process in cementitious materials.

### **3.3.2.3 Establishment of the carbonation profile with optical fibre Raman platform**

Using the  $\nu_1$  CO<sub>3</sub> peak height as the indicator, the carbonation profiles obtained from the optical fibre Raman platform was plotted together with those obtained by bench-mounted Raman spectroscopy and TG in Fig. 16. Apparently, the calcium carbonate profiles obtained from these three techniques are highly comparable. As TG has been regarded as a reliable technique for quantifying the calcium carbonate formed during the carbonation of cementitious materials, the above results suggest that the ‘coaxial’ optical fibre Raman system as established in the current study can adequately differentiate the variation of calcium carbonate content in carbonated PC paste over the depth from the surface of concrete and, hence, offers a good potential for monitoring the carbonation of concrete in future.

### **3.4 Comparison of the SNR of spectra from two Raman systems**

The carbonation profile has been successfully established by the ‘coaxial’ optical fibre Raman system, with the results being well corroborated by the bench-mounted Raman spectroscopy and TG. However, by comparing Fig. 6 and Fig. 7, it is apparent that the peak intensity (i.e., signal level) and noise level of the Raman spectra were dramatically different between these two



Raman systems, e.g., the signal intensities of Raman peaks retrieved from optical fibre Raman system were lower than those from bench-mounted Raman spectroscopy. Hence, in an attempt to compare the quality of the spectra obtained from these two Raman systems and also to understand the potential issues which could have been caused by optical fibre Raman pathway, the signal level, noise level and SNR values of the Raman spectra obtained at the depth of 0-2 mm were calculated and compared. As  $\nu_1$  CO<sub>3</sub> band is the most intense Raman peak, it was thus employed as the reference for the calculation and the results are reported in Table 7.

From Table 7, the following two features can be clearly observed:

- i) Signal and noise. Both the signal intensity and the noise level of the  $\nu_1$  CO<sub>3</sub> band from optical fibre Raman system were much lower than those from bench-mounted Raman spectroscopy, respectively.
- ii) SNR. It is evident that, due to the huge difference in the signal intensities between these two Raman systems, even though the noise level of the fibre mode was lower than that of bench-mounted Raman system, the overall SNR of the Raman spectra collected under the optical fibre Raman system (9.3) was still much lower than that of the bench-mounted Raman spectroscopy (81.0), i.e., around 9 times difference. This reduced SNR values of spectra retrieved under optical fibre Raman system could be caused by the different optical set-up between these two Raman systems, such as the alignment of the fibre optics in the fibre pathway. Besides, the lower power density of excitation in the optical fibre Raman system, as well as the inhomogeneous nature of the PC-bearing matrix, could decrease excitation efficiency of the fibre mode. The reduced SNR from optical fibre Raman spectrometer suggest that, further researches, such as the optical fibre

system optimisation and the signal enhancement, are required to achieve high signal level to recognise some trace level elements from cementitious materials.

## **Conclusions**

A bespoke Raman spectroscopy based ‘coaxial’ optical fibre sensing platform with 514.5nm excitation laser was successfully developed in this study for detecting the carbonation product formed in a pure PC paste. This optical fibre platform enabled the transmission of excitation laser through an optical fibre and the collection of Raman signal through the other optical fibre. The optical fibre Raman system has demonstrated, both qualitatively and quantitatively, its capacity in characterising the calcium carbonate polymorphs and its profile formed during the carbonation of a PC paste. The carbonation profile established with the optical fibre Raman system is highly comparable with that from the TG analysis, showing its good potential as a future sensor system for monitoring the health condition and the performance of concrete structures. However, issues such as insufficient sensitivity, weak signal and small spot size, together with appropriate package for the rather sophisticated optics, still need to be addressed in future studies before a Raman spectroscopy-based optical fibre sensor network could be eventually developed for real civil engineering applications.

## **Acknowledgements**

The authors would like to thank the EPSRC UK-China Science Bridge project (EP/G042594/1), China Scholarship Council and UCL Faculty of Engineering Sciences for supporting Yanfei Yue's PhD study. The funding from the QualityNano Transnational Access Project and the UK Royal Society International Exchange Scheme with Ireland (IE131481) are also gratefully acknowledged. The CEM I Portland cement used in this research was supplied by QUINN Group.

## References

- [1] P. Moyo, J. Brownjohn, R. Suresh, S. Tjin, Development of fiber Bragg grating sensors for monitoring civil infrastructure, *Eng. Struct.* 27 (2005) 1828-1834.
- [2] S. Liehr, P. Lenke, M. Wendt, K. Krebber, M. Seeger, E. Thiele, H. Metschies, B. Gebreselassie, J.C. Munich, Polymer optical fiber sensors for distributed strain measurement and application in structural health monitoring, *IEEE. Sensors. J.* 9 (2009) 1330-1338.
- [3] A.M. Neville, *Properties of Concrete*, fifth ed., Prentice Hall, San Francisco, 1995.
- [4] J.P. Broomfield, Carbonation and its effects in reinforced concrete, *Mater. Performance.* 39 (2000) 64-67.
- [5] T.F. Sevelsted, J. Skibsted, Carbonation of C-S-H and C-A-S-H samples studied by  $^{13}\text{C}$ ,  $^{27}\text{Al}$  and  $^{29}\text{Si}$  MAS NMR spectroscopy, *Cem. Concr. Res.* 71 (2015) 56-65.
- [6] B. Lagerblad, *Carbon dioxide uptake during concrete life cycle—state of the art*, Swedish Cement and Concrete Research Institute CBI, Stockholm, 2005.
- [7] Q. Zhou, F.P. Glasser, Kinetics and mechanism of the carbonation of ettringite, *Adv. Cem. Res.* 12 (2000) 131-136.

- [8] G.W. Groves, A. Brough, I.G. Richardson, C.M. Dobson, Progressive changes in the structure of hardened  $C_3S$  cement pastes due to carbonation, *J Am Ceram Soc.* 74 (1991) 2891-2896.
- [9] V. Papadakis, M. Fardis, C. Vayenas, Effect of composition, environmental factors and cement-lime mortar coating on concrete carbonation, *Mater. Struc.* 25 (1992) 293-304.
- [10] J.P. Broomfield, *Corrosion of Steel in Concrete: Understanding, Investigation and Repair*, second ed., Taylor & Francis, Abingdon, 2007.
- [11] I. Richardson, The nature of CSH in hardened cements, *Cem. Concr. Res.* 29 (1999) 1131-1147.
- [12] A. Morandau, M. Thiery, P. Dangla, Investigation of the carbonation mechanism of CH and CSH in terms of kinetics, microstructure changes and moisture properties, *Cem. Concr. Res.* 56 (2014) 153-170.
- [13] Z. Šauman, Carbonization of porous concrete and its main binding components, *Cem. Concr. Res.* 1 (1971) 645-662.
- [14] Y.F. Houst, F.H. Wittmann, Depth profiles of carbonates formed during natural carbonation, *Cem. Concr. Res.* 32 (2002) 1923-1930.
- [15] G. Villain, M. Thiery, G. Platret, Measurement methods of carbonation profiles in concrete: Thermogravimetry, chemical analysis and gammadensimetry, *Cem. Concr. Res.* 37 (2007) 1182-1192.
- [16] D. McPolin, P. Basheer, A. Long, Carbonation and pH in mortars manufactured with supplementary cementitious materials, *J. Mater. Civil. Eng.* 21 (2009) 217-225.

- [17] M.-T. Liang, R. Huang, S.-A. Fang, Carbonation service life prediction of existing concrete viaduct/bridge using time-dependent reliability analysis, *J. Mar. Sci. Technol.* 21 (2013) 94-104.
- [18] C.-F. Chang, J.-W. Chen, The experimental investigation of concrete carbonation depth, *Cem. Concr. Res.* 36 (2006) 1760-1767.
- [19] H.J. Lee, D.G. Kim, J.H. Lee, M.S. Cho, A study for carbonation degree on Concrete using a phenolphthalein indicator and fourier-transform infrared spectroscopy, *Int. J. Civ. Environ. Eng.* 34 (2012) 184-190.
- [20] M. Thiery, G. Villain, P. Dangla, G. Platret, Investigation of the carbonation front shape on cementitious materials: Effects of the chemical kinetics, *Cem. Concr. Res.* 37 (2007) 1047-1058.
- [21] G. Villain, M. Thiery, Gammadensimetry: A method to determine drying and carbonation profiles in concrete, *NDT & E Int.* 39 (2006) 328-337.
- [22] TC56 RILEM, CPC-18 Measurement of hardened concrete carbonation depth, *Mater Struct.* 126 (1988) 453-455.
- [23] N.R. Buenfeld, N.M. Hassanein, A.J. Jones, An artificial neural network for predicting carbonation depth in concrete structures, *Manuals and Reports on Engineering Practice*, 1998, 77-117.
- [24] A.B. Poole, I. Sims, *Concrete Petrography: A Handbook of Investigative Techniques*, second ed., Taylor & Francis, Boca Raton, 2015.
- [25] L. Parrott, A review of carbonation in reinforced concrete, C and CA report for Building Research Establishment, Watford, UK, 1987.

- [26] Y. Lo, H. Lee, Curing effects on carbonation of concrete using a phenolphthalein indicator and Fourier-transform infrared spectroscopy, *Build. Environ.* 37 (2002) 507-514.
- [27] J.J. Chang, W. Yeih, R. Huang, C.T. Chen, Suitability of several current used concrete durability indices on evaluating the corrosion hazard for carbonated concrete, *Mater. Chem. Phys.* 84 (2004) 71-78.
- [28] M. Thiéry, P. Faure, A. Morandea, G. Platret, J.-F. Bouteloup, P. Dangla, V. Baroghel-Bouny, Effect of carbonation on the microstructure and moisture properties of cement-based materials, In: 12th International Conference on Durability of Building Materials and Components (XII DBMC), Porto, Portugal, 12-15 Apr 2011, pp. 1-8. FEUP.
- [29] M. Arandigoyen, B. Bicer-Simsir, J.I. Alvarez, D.A. Lange, Variation of microstructure with carbonation in lime and blended pastes, *Appl. Surf. Sci.* 252 (2006) 7562-7571.
- [30] M.P. Basheer, K.T. Grattan, T. Sun, A.E. Long, D. McPolin, W. Xie, Fiber optic chemical sensor systems for monitoring pH changes in concrete, In: *Advanced Environmental, Chemical, and Biological Sensing Technologies II* (SPIE Vol. 5586), Philadelphia, PA, 25 Oct 2004, pp. 144-153. Bellingham: SPIE.
- [31] J.M. Ko, Y.Q. Ni, Technology developments in structural health monitoring of large-scale bridges, *Eng. Struct.* 27 (2005) 1715-1725.
- [32] W. McCarter, T. Chrisp, A. Butler, P. Basheer, Near-surface sensors for condition monitoring of cover-zone concrete, *Constr. Build. Mater.* 15 (2001) 115-124.
- [33] W. McCarter, M. Emerson, H. Ezirim, Properties of concrete in the cover zone: developments in monitoring techniques, *Mag. Concrete. Res.* 47 (1995) 243-251.

- [34] D. Chen, X. Cheng, Hydrostatic pressure sensor based on a gold-coated fiber modal interferometer using lateral offset splicing of single mode fiber, *Prog. Electromagn. Res.* 124 (2012) 315-329.
- [35] B.P. Pal, *Fundamentals of Fibre Optics in Telecommunication and Sensor Systems*, New Age International Ltd, Delhi, 1992.
- [36] D.O. McPolin, P. Basheer, A.E. Long, W. Xie, T. Sun, K.T. Grattan, Development and longer term in situ evaluation of fiber-optic sensors for monitoring of structural concrete, *IEEE. Sensors. J.* 9 (2009) 1537-1545.
- [37] W. Xie, T. Sun, K.T. Grattan, D. McPolin, P. Basheer, A.E. Long, Fibre optic chemical sensor systems for internal concrete condition monitoring, In: *Second European Workshop on Optical Fibre Sensors (SPIE Vol. 5502)*, Santander, Spain, 09 Jun 2004, pp. 334-337. Bellingham: SPIE.
- [38] G. Badini, K. Grattan, A. Tseung, Impregnation of a pH-sensitive dye into sol-gels for fibre optic chemical sensors, *Analyst.* 120 (1995) 1025-1028.
- [39] R.D. Davies, N.R. Buenfeld, *Automated monitoring of the deterioration of concrete structures*, Department of Trade and Industry, London, 2007.
- [40] M. RAUPACH, P. SCHIEßL, Monitoring system for the penetration of chlorides, carbonation and the corrosion risk for the reinforcement. *Constr. Build. Mater.* 11 (1997) 207-214.
- [41] M. RAUPACH, P. SCHIEßL, Macrocell sensor systems for monitoring of the corrosion risk of the reinforcement in concrete structures. *NDT & E Int.* 34 (2001) 435-442.
- [42] D.A. Long, *Raman Spectroscopy*, McGraw-Hill International Book Company, New York, 1977.

- [43] J. Bensted, Uses of Raman spectroscopy in cement chemistry, *J. Am. Ceram. Soc.* 59 (1976) 140-143.
- [44] D. Bonen, T. Johnson, S. Sarkar, Characterization of principal clinker minerals by FT-Raman microspectroscopy, *Cem. Concr. Res.* 24 (1994) 959-965.
- [45] L. Black, C. Breen, J. Yarwood, J. Phipps, G. Maitland, In situ Raman analysis of hydrating C<sub>3</sub>A and C<sub>4</sub>AF pastes in presence and absence of sulphate, *Adv. Appl Ceram.* 105 (2006) 209-216.
- [46] S. Martinez-Ramirez, M. Frías, C. Domingo, Micro-Raman spectroscopy in white portland cement hydration: long-term study at room temperature, *J. Raman. Spectrosc.* 37 (2006) 555-561.
- [47] R.J. Kirkpatrick, J. Yarger, P.F. McMillan, Y. Ping, X. Cong, Raman spectroscopy of CSH, tobermorite, and jennite, *Adv. Cem. Based. Mater.* 5 (1997) 93-99.
- [48] K. Garbev, P. Stemmermann, L. Black, C. Breen, J. Yarwood, B. Gasharova, Structural features of C–S–H (I) and its carbonation in air—a Raman spectroscopic study. Part I: fresh phases, *J. Am. Ceram. Soc.* 90 (2007) 900-907.
- [49] I. Richardson, J. Skibsted, L. Black, R.J. Kirkpatrick, Characterisation of cement hydrate phases by TEM, NMR and Raman spectroscopy, *Adv. Cem. Res.* 22 (2010) 233-248.
- [50] S. Martinez-Ramirez, S. Sanchez-Cortes, J. Garcia-Ramos, C. Domingo, C. Fortes, M. Blanco-Varela, Micro-Raman spectroscopy applied to depth profiles of carbonates formed in lime mortar, *Cem. Concr. Res.* 33 (2003) 2063-2068.
- [51] C. Gabrielli, R. Jaouhari, S. Joiret, G. Maurin, In situ Raman spectroscopy applied to electrochemical scaling. Determination of the structure of vaterite, *J. Raman. Spectrosc.* 31 (2000) 497-501.



- [52] L. Black, C. Breen, J. Yarwood, K. Garbev, P. Stemmermann, B. Gasharova, Structural Features of C–S–H(I) and Its Carbonation in Air—A Raman Spectroscopic Study. Part II: Carbonated Phases, *J. Am. Ceram. Soc.* 90 (2007) 908-917.
- [53] M. Tlili, M.B. Amor, C. Gabrielli, S. Joiret, G. Maurin, P. Rousseau, Characterization of CaCO<sub>3</sub> hydrates by micro-Raman spectroscopy, *J. Raman. Spectrosc.* 33 (2002) 10-16.
- [54] J. Corvisier, F. Brunet, A. Fabbri, S. Bernard, N. Findling, G. Rimmelé, V. Barlet-Gouédard, O. Beyssac, B. Goffé, Raman mapping and numerical simulation of calcium carbonates distribution in experimentally carbonated Portland-cement cores, *Eur. J. Mineral.* 22 (2010) 63-74.
- [55] H. Rutt, J. Nicola, Raman spectra of carbonates of calcite structure, *J. Physics. C: Solid. State.* 7 (1974) 4522.
- [56] J. Bensted, Raman spectral studies of carbonation phenomena, *Cem. Concr. Res.* 7 (1977) 161-164.
- [57] U. Wehrmeister, A. Soldati, D. Jacob, T. Häger, W. Hofmeister, Raman spectroscopy of synthetic, geological and biological vaterite: a Raman spectroscopic study, *J. Raman. Spectrosc.* 41 (2010) 193-201.
- [58] J. Ibáñez, L. Artús, R. Cuscó, Á. López, E. Menéndez, M.C. Andrade, Hydration and carbonation of monoclinic C<sub>2</sub>S and C<sub>3</sub>S studied by Raman spectroscopy, *J. Raman. Spectrosc.* 38 (2007) 61-67.
- [59] M.G. Shim, B.C. Wilson, Development of an in vivo Raman spectroscopic system for diagnostic applications, *J. Raman. Spectrosc.* 28 (1997) 131-142.
- [60] J.T. Motz, M. Hunter, L.H. Galindo, J.A. Gardecki, J.R. Kramer, R.R. Dasari, M.S. Feld, Optical fiber probe for biomedical Raman spectroscopy, *Appl. Optics.* 43 (2004) 542-554.

- [61] C. Wang, T.J. Vickers, J.B. Schlenoff, C.K. Mann, In situ monitoring of emulsion polymerization using fiber-optic Raman spectroscopy, *Appl. Spectrosc.* 46 (1992) 1729-1731.
- [62] J.F. Aust, K.S. Booksh, M.L. Myrick, Novel in situ probe for monitoring polymer curing, *Appl. Spectrosc.* 50 (1996) 382-387.
- [63] M. Myrick, J. Kolis, E. Parsons, K. Chike, M. Lovelace, W. Scrivens, R. Holliday, M. Williams, In situ fiber-optic Raman spectroscopy of organic chemistry in a supercritical water reactor, *J. Raman. Spectrosc.* 25 (1994) 59-65.
- [64] W.C. Bell, K.S. Booksh, M. Myrick, Monitoring anhydride and acid conversion in supercritical/hydrothermal water by in situ fiber-optic Raman spectroscopy, *Anal. Chem.* 70 (1998) 332-339.
- [65] Y. Yue, Y. Bai, P.M. Basheer, J.J. Boland, J.J. Wang, Monitoring the cementitious materials subjected to sulfate attack with optical fiber excitation Raman spectroscopy, *Opt. Eng.* 52 (2013) 104107-1 - 104107-10.
- [66] Y. Yue, J.J. Wang, P.A.M. Basheer, J.J. Boland, Y. Bai, Characterisation of carbonated Portland cement paste with optical fibre excitation Raman spectroscopy, *Constr. Build. Mater.* 135 (2017) 369-376.
- [67] BSEN 197-1: 2011, Cement, Composition, Specifications and Conformity Criteria for Common Cements, British Standard Institution (BSI), London, 2011.
- [68] C.J. Strachan, D. Pratiwi, K.C. Gordon, T. Rades, Quantitative analysis of polymorphic mixtures of carbamazepine by Raman spectroscopy and principal components analysis, *J. Raman. Spectrosc.* 35 (2004) 347-352.

- [69] ASTM E 579-04:2015, Standard Test Method for Limit of Detection of Fluorescence of Quinine Sulfate in Solution, ASTM International, 2015.
- [70] M. Földvári, Handbook of thermogravimetric system of minerals and its use in geological practice, 2011.
- [71] M.M. Carrabba, K.M. Spencer, R.B. Edmonds, R.D. Rauh, J.W. Haas III, Spectroelectrochemical technologies and instrumentation for environmental and process monitoring, In: Environmental and Process Monitoring Technologies (SPIE Vol. 1637), Los Angeles, CA, 19 Jan 1992, pp. 82-90. SPIE.
- [72] M.M. Carrabba, R.D. Rauh, Apparatus for measuring Raman spectra over optical fibers, Patent 5112127-A, USA, 1992.
- [73] M. Myrick, S. Angel, Elimination of background in fiber-optic Raman measurements, *Appl. Spectrosc.* 44 (1990) 565-570.
- [74] R.L. McCreery, Raman Spectroscopy for Chemical Analysis, John Wiley & Sons, USA, 2005.
- [75] R.L. McCreery, M. Fleischmann, P. Hendra, Fiber optic probe for remote Raman spectrometry, *Anal. Chem.* 55 (1983) 146-148.
- [76] I.R. Lewis, P.R. Griffiths, Raman spectrometry with fiber-optic sampling, *Appl. Spectrosc.* 50 (1996) 12A-30A.
- [77] C.L. Schoen, T.F. Cooney, S.K. Sharma, D.M. Carey, Long fiber-optic remote Raman probe for detection and identification of weak scatterers, *Appl. Optics.* 31 (1992) 7707-7715.
- [78] M.L. Myrick, S.M. Angel, R. Desiderio, Comparison of some fiber optic configurations for measurement of luminescence and Raman scattering, *Appl. Optics.* 29 (1990) 1333-1344.

- [79] J. May, Y.-S. Li, Fiber Raman background study and its application in setting up optical fiber Raman probes, *Appl. Optics*. 35 (1996) 2527-2533.
- [80] Y. Yue. Application of optical fibre Raman spectroscopy for characterising carbonation and chloride attack of cementitious materials, Doctoral dissertation, 2015, University College London.
- [81] T. Ohsaka, F. Izumi, Y. Fujiki, Raman spectrum of anatase,  $\text{TiO}_2$ , *J. Raman. Spectrosc.* 7 (1978) 321-324.
- [82] H.G.M. Edwards, S.E. Jorge Villar, J. Jehlicka, T. Munshi, FT-Raman spectroscopic study of calcium-rich and magnesium-rich carbonate minerals, *Spectrochim. Acta. A Mol. Biomol. Spectrosc.* 61(2005) 2273-2280.
- [83] P. Prasad, A. Pradhan, T. Gowd, In situ micro-Raman investigation of dehydration mechanism in natural gypsum, *Curr. Sci.* 80 (2001) 1203-1207.
- [84] C.-Y. Tsao, J.W. Weber, P. Campbell, P.I. Widenborg, D. Song, M.A. Green, Low-temperature growth of polycrystalline Ge thin film on glass by in situ deposition and ex situ solid-phase crystallization for photovoltaic applications, *Appl. Surf. Sci.* 255 (2009) 7028-7035.

### Author biography

### Author Biographies

**Yanfei Yue** is currently a Lecturer in Materials in the College of Materials Science and Engineering at Chongqing University, China. She received her PhD degree in Civil Engineering from University College London (UK), UK, and BSc & MSc degrees in Building Materials from Chongqing University. Her

research lies in the development and application of advanced sensor technology for monitoring concrete structures, and novel, sustainable cementitious materials. She is a Corporate member of The Institute of Concrete Technology (ICT), UK.

**Jing Jing Wang** is a senior researcher in CRANN at Trinity College Dublin. Prior to that, he carried out his postdoctoral researches in the University of Sheffield. He received his PhD degree in physics from the University of Leeds in 2005. He earned his MSc degree in physics from Peking University in 1998 and received his BEng degree in optical engineering from Tsinghua University in 1990. He has authored more than 80 refereed publications and his current research interests include Raman spectroscopy, fluorescence spectroscopy, near-field optics and nano-photonics.

**P. A. Muhammed Basheer** is the Head of School of Civil Engineering and Professor of Structural Engineering, University of Leeds, England, UK. He is also a visiting professor at Zhejiang University and Chongqing University in China. He received his bachelor's degree in civil engineering and master's degree in structural engineering, both from India and PhD in structural materials from Queen's University Belfast. He has been an educationalist and researcher in the field of civil (structural) engineering for more than 30 years. His research interests are primarily on the Science, Technology and Performance of Concrete and Concrete Structures, with special emphasis on nondestructive evaluation, structural health monitoring and performance testing of concrete structures. He is an elected fellow of the Irish Academy of Engineering, Institution of Civil Engineers and American Concrete Institute. He is also a member of numerous technical committees of both the American Concrete Institute and RILEM. He is an editor of the International Journal of Construction and Building Materials and an associate editor of the International Journal of Civil Structural Health Monitoring. He has authored more than 300 refereed technical publications and received the American Concrete Institute's ACI/James Instruments Award for best NonDestructive Testing Limited in 1990 for developing the Autoclam Permeability System and in 1999 for developing the Permit Ion Migration test.

**John J. Boland** received a BSc degree in chemistry from University College Dublin and a PhD in chemical physics from the California Institute of Technology. From 1984 to 1994 he was a member of the research staff at the IBM T.J. Watson Research Center (New York). In 1994, he joined the chemistry faculty at the University of North Carolina at Chapel Hill where he was appointed the J.J. Hermans Chair Professor of Chemistry and Applied and Materials Science. In 2002, he moved to the School of Chemistry at Trinity College Dublin as a Science Foundation Ireland Principal Investigator. In 2005, he was appointed as a director of the Centre for Research on Adaptive Nanostructures and Nanodevices (CRANN), which is Ireland's flagship nano and materials science institute. He is an internationally recognised expert in the chemistry of semiconductor surfaces and the use of scanning probe microscopy to elucidate materials and device properties. He was elected a fellow of Trinity College in 2008, a fellow of the American Vacuum Society (AVS) in 2009 and a fellow of the American Association for the Advancement of Science (AAAS) in 2010. He was the recipient of ACSIN Nanoscience Prize in 2011, St Petersburg, Russia and an ERC Advanced Grant.

**Yun Bai** is Reader in Materials, Deputy Head of Civil Engineering Section and the Head of the Advanced and Innovative Materials (AIM) research group in the Department of Civil, Environmental and Geomatic Engineering (CEGE) at University College London (UCL), UK. He received his BSc degree in building materials from Chongqing University, China, a MSc in computing and information systems (Distinction) from University of Ulster, UK and a PhD in construction materials from Queen's University Belfast, UK. Prior to his MSc and PhD studies in the UK in 2000, he was an associate civil engineer/civil engineer and project manager in China for over 7 years. After his PhD study in 2004, he worked as a post-doctoral research associate in The University of Sheffield and then joined Queen's University Belfast as a Lecturer in Civil Engineering in 2007 before taking a Senior Lecturer post in UCL in early 2012. His current

research profile can be summarized as ‘industry driven and interdisciplinary,’ which covers a wide range of material science and engineering properties of materials including novel low-carbon cement and concrete, concrete durability, nuclear waste immobilization, structural health monitoring and nondestructive testing of structural concrete. He is a member of The Institute of Concrete Technology and a member of the Cementitious Materials Group Committee, The Institute of Materials, Minerals and Mining (IOM<sup>3</sup>).

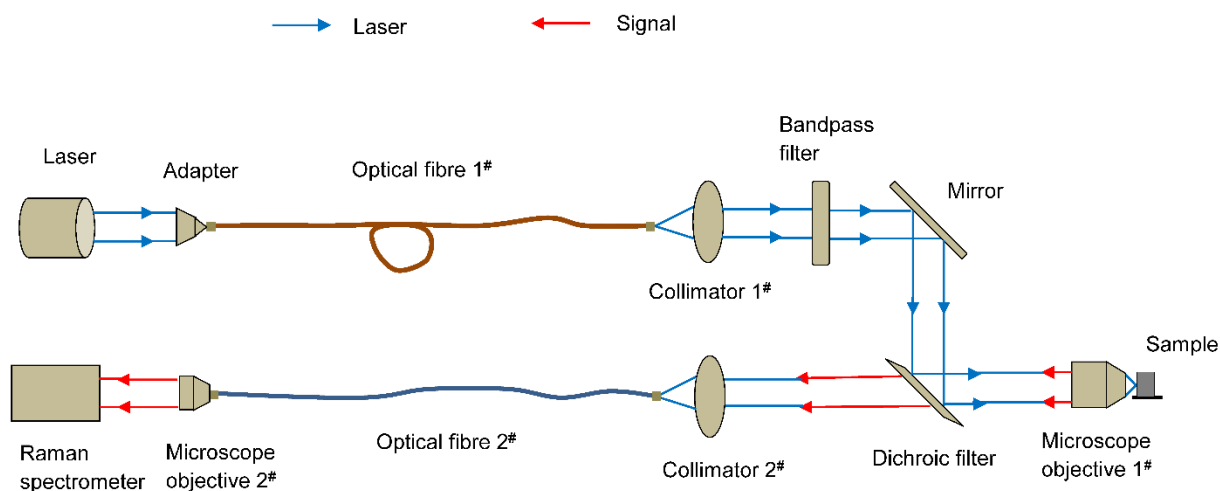


**Fig. 1 Schematic diagram of the ‘coaxial’ optical fibre sensing platform based on Raman spectroscopy.**

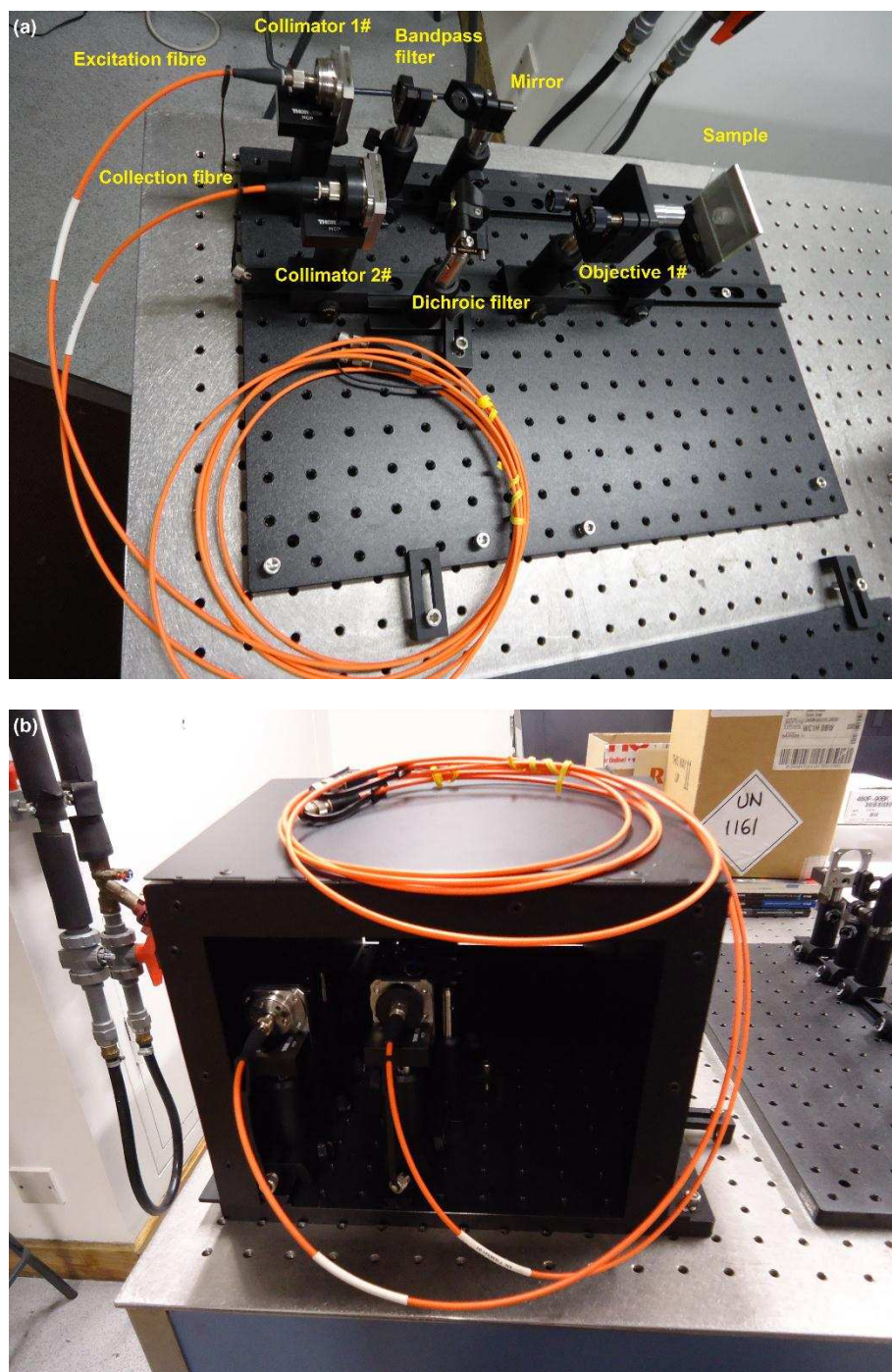


**Fig. 2 Optical fibre sensing platform established. (a) without optical enclosure. (b) with optical enclosure.**

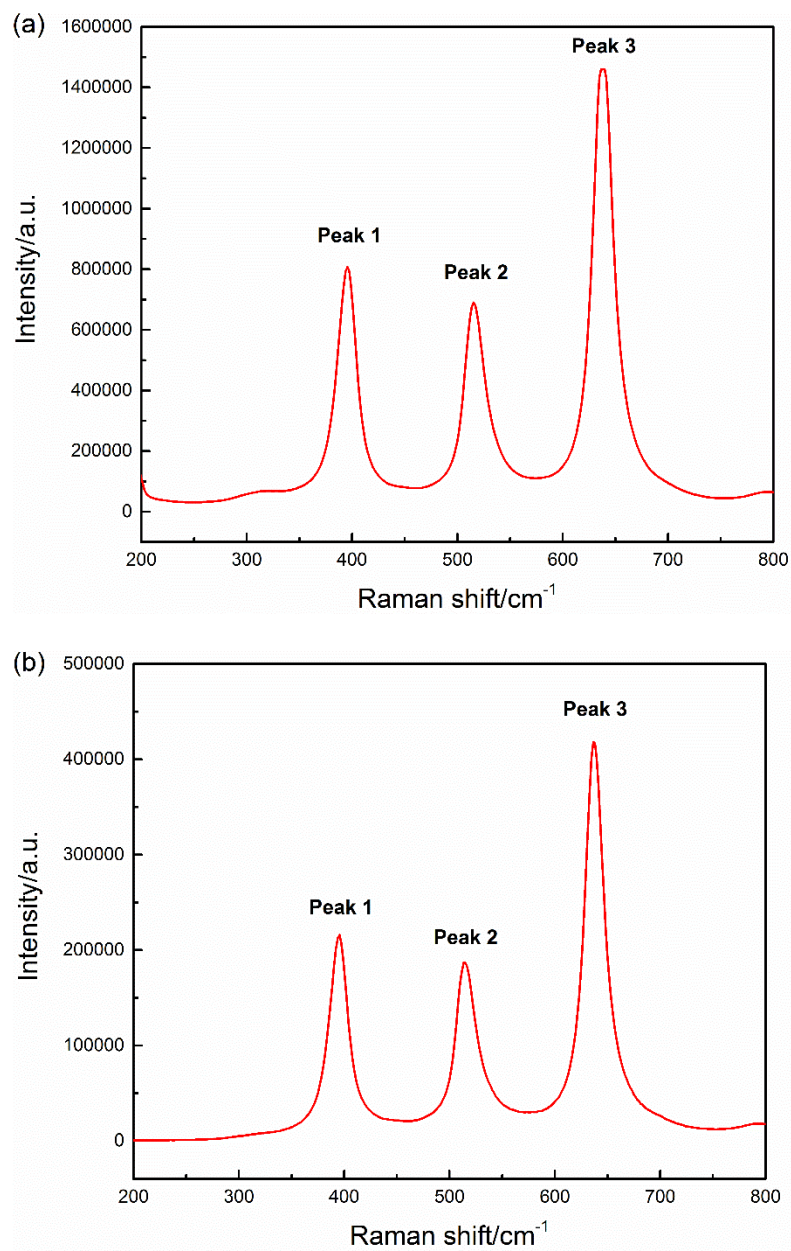


**Fig. 3 Raman spectra of  $\text{TiO}_2$ . (a) Bench-mounted Raman system. (b) Optical fibre Raman system.**



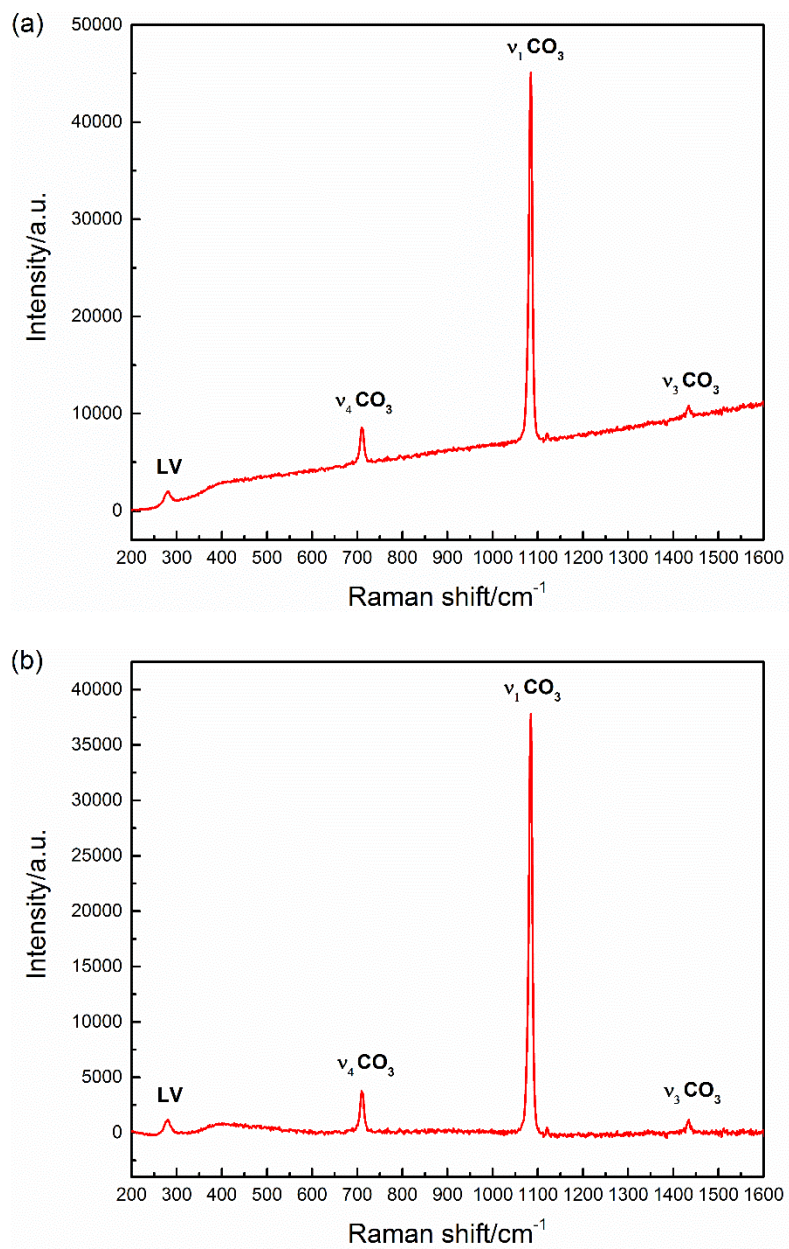


**Fig. 4 Optical fibre Raman spectra of  $\text{CaCO}_3$ . (a) Original spectrum. (b) Spectrum after subtracting background.**

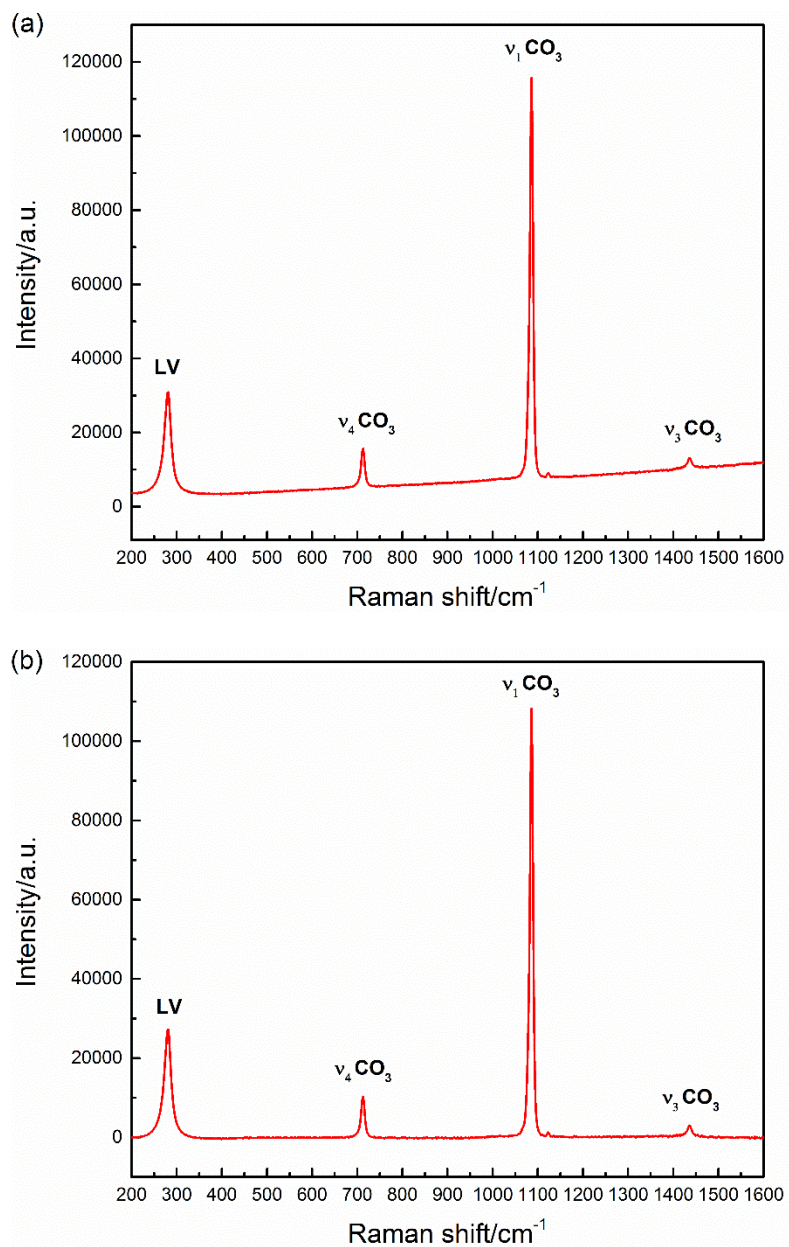


**Fig. 5 Bench-mounted Raman spectra of  $\text{CaCO}_3$ . (a) Original spectrum. (b) Spectrum after subtracting background.**

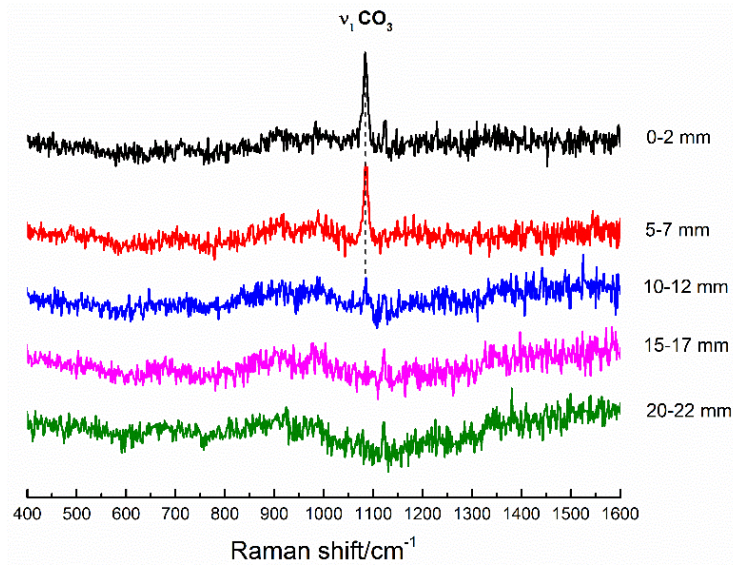


**Fig. 6** Optical fibre Raman spectra of PC paste samples collected at five depths.

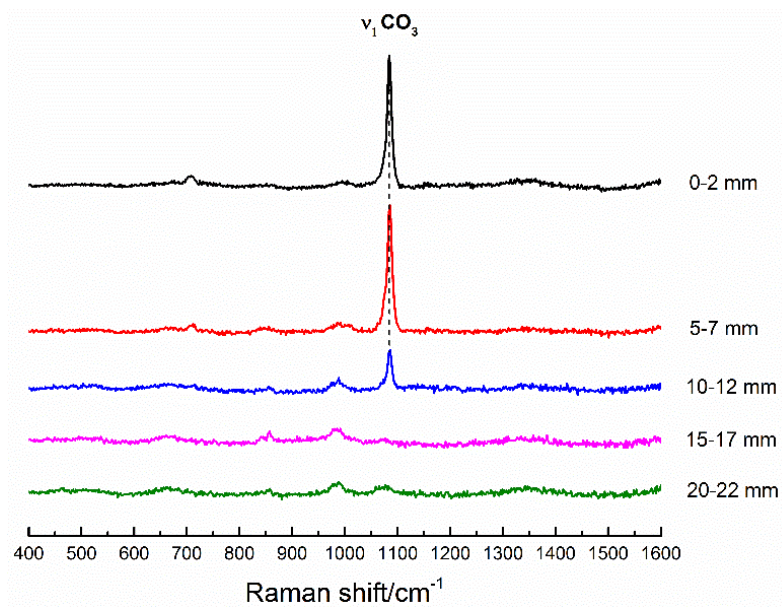


**Fig. 7 Bench-mounted Raman spectra of PC paste samples collected at five depths.**

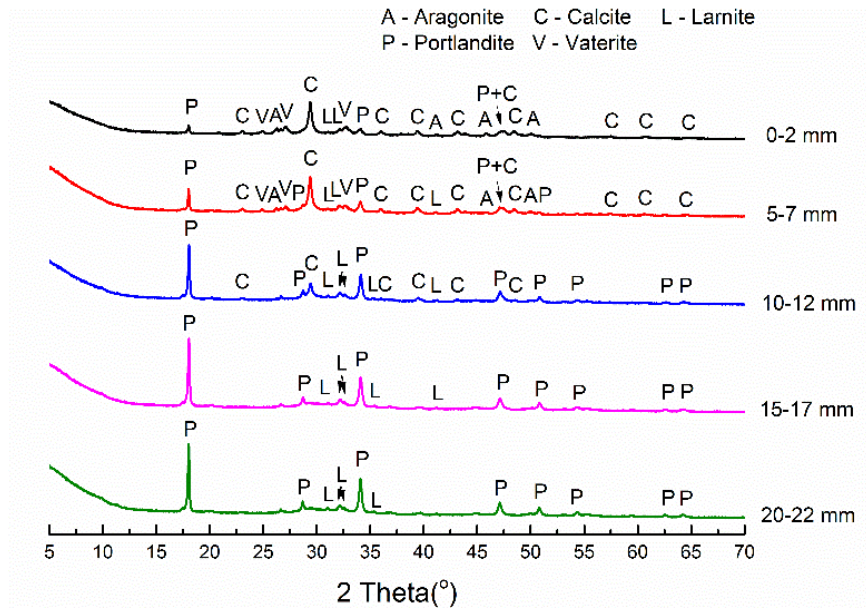


**Fig. 8 XRD patterns of PC paste samples collected at five depths.**

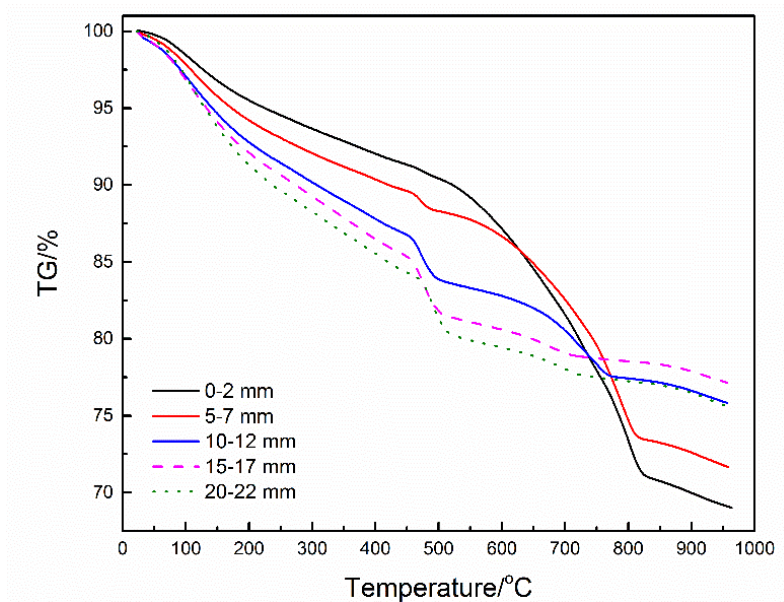


**Fig. 9** TG curves of PC paste samples collected at five depths.

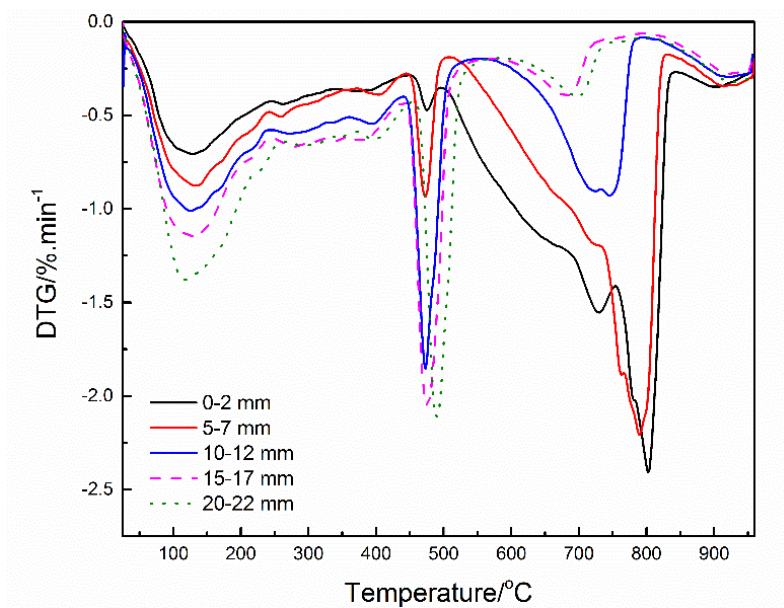


**Fig. 10** DTG curves of PC paste samples collected at five depths.

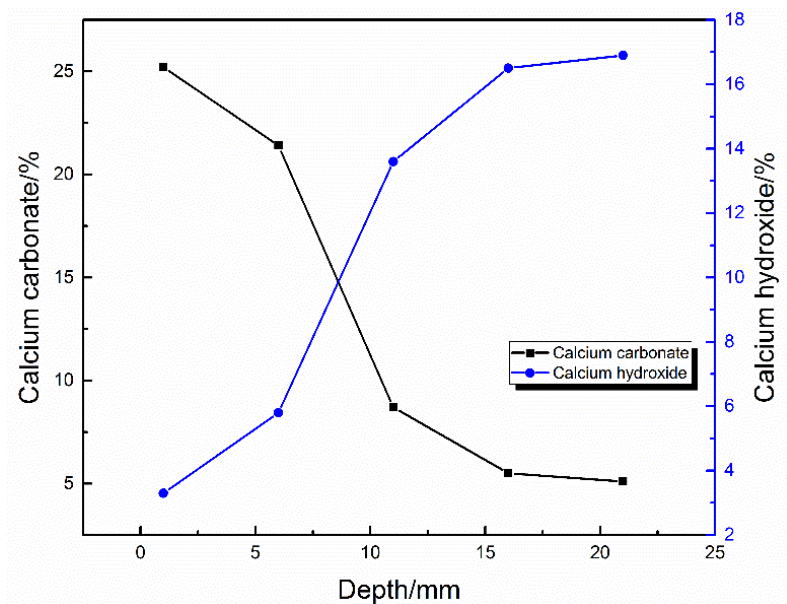
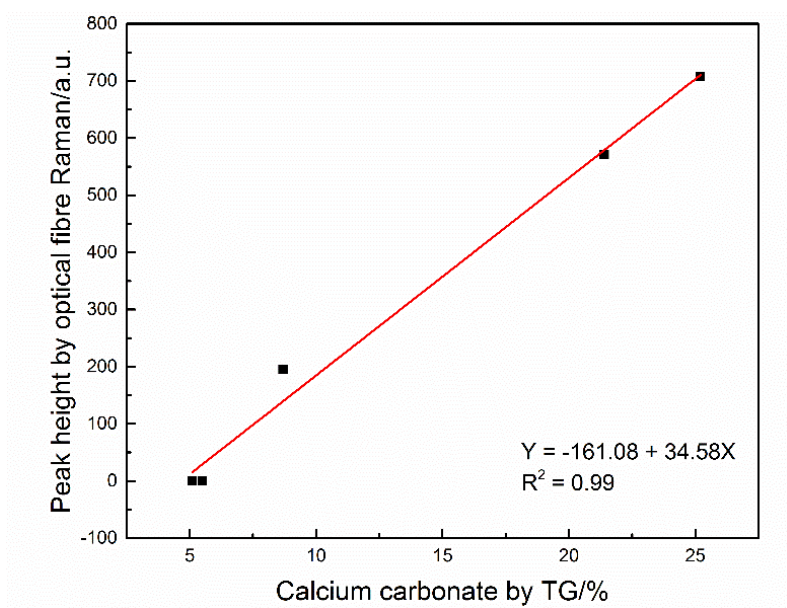
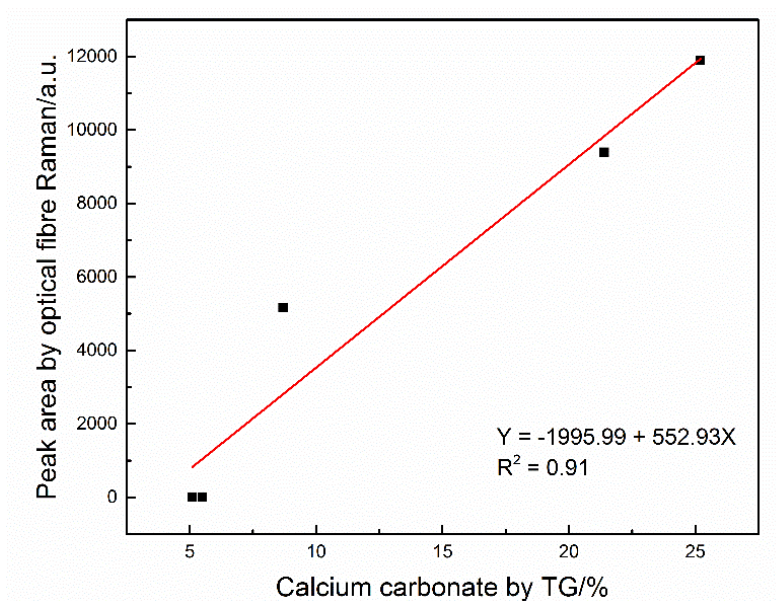


Fig. 11 The profiles of  $\text{CaCO}_3$  and  $\text{Ca(OH)}_2$  in PC paste measured by TG.



**Fig. 12 Correlation between TG and peak height obtained from PC paste samples under optical fibre Raman system.**



**Fig. 13 Correlation between TG and peak area obtained from PC paste samples under optical fibre Raman system.**

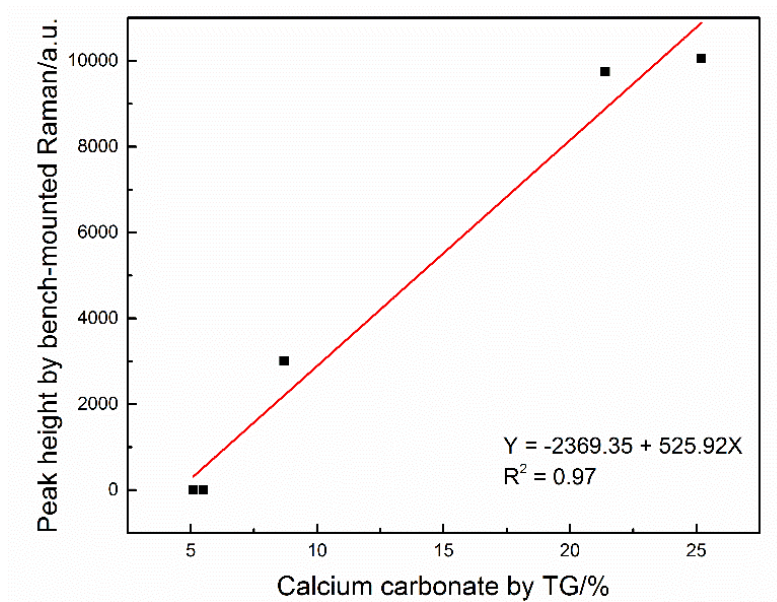


**Fig. 14 Correlation between TG and peak height obtained from PC paste samples under bench-mounted Raman system.**



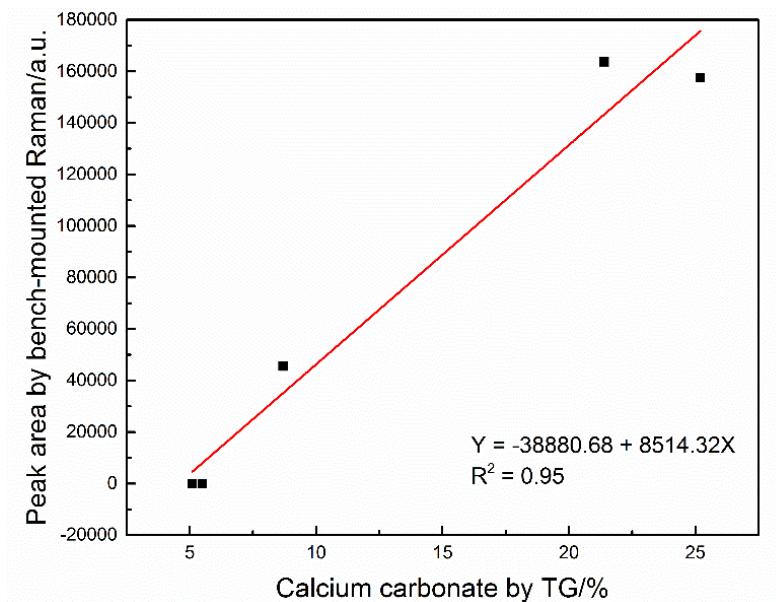


**Fig. 15 Correlation between TG and peak area obtained from PC paste samples under bench-mounted Raman system.**

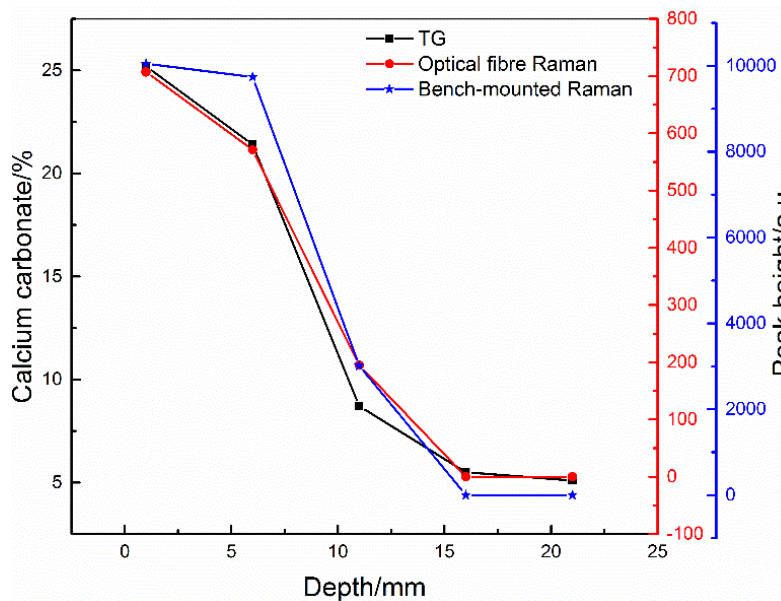


**Fig. 16 Carbonation profiles established by optical fibre Raman system, TG and bench-mounted Raman system.**

**Table 1. Chemical composition of Portland cement.**

	SiO <sub>2</sub>	Al <sub>2</sub> O <sub>3</sub>	Fe <sub>2</sub> O <sub>3</sub>	CaO	MgO	K <sub>2</sub> O	Na <sub>2</sub> O	SO <sub>3</sub>
% wt	23.00	6.15	2.95	61.30	1.80	0.68	0.22	2.50

**Table 2. Raman bands and assignments of TiO<sub>2</sub> under bench-mounted Raman and optical fibre Raman systems.**

	Raman shift/ cm <sup>-1</sup>		
	Peak 1	Peak 2	Peak 3
Bench-mounted Raman system	395	517	638
Optical fibre Raman system	395	516	638

**Table 3. Laser power at different locations of the optical fibre Raman and bench-mounted Raman systems.**

	Locations measured	Power (mW)	Transmission/coupling efficiency (%)	Excitation spot area (μm <sup>2</sup> )	Excitation power density (mW/μm <sup>2</sup> )
Optical fibre Raman system	Laser output	15.6	100	27.33	0.38
	Optical fibre 1#	14.1	90		

	Collimator 1#	13.4	86		
	Bandpass filter	13.1	84		
	Mirror	11.6	74		
	Dichroic filter	11.4	73		
	Objective 1#	10.4	67		
Bench-mounted	Laser output	15.6	100		
Raman system	Objective	3.2	21	4.95	0.65

**Table 4. Raman bands and assignments of CaCO<sub>3</sub> under optical fibre Raman and bench-mounted Raman systems.**

	Optical fibre Raman system	Bench-mounted Raman system	Assignments
Raman shift /cm <sup>-1</sup>	1084	1086	Symmetric stretching ( $\nu_1$ ) of CO <sub>3</sub> in calcite
	1434	1436	Asymmetric stretching ( $\nu_3$ ) of CO <sub>3</sub> in calcite
	711	712	In-plane bending ( $\nu_4$ ) of CO <sub>3</sub> in calcite
	280	280	Lattice vibration (LV) in calcite

**Table 5 Summary of the Raman peak features of PC paste samples under optical fibre Raman system and TG quantified CaCO<sub>3</sub>.**

	Wavenumber	Height	Area	Total CaCO <sub>3</sub> by TG (%)
0-2 mm	1084.4	707.4	11895.0	25.2
5-7 mm	1085.3	571.3	9395.3	21.4
10-12 mm	1085.1	195.0	5167.6	8.7
15-17 mm	0	0	0	5.5
20-22 mm	0	0	0	5.1

**Table 6 Summary of the Raman peak features of PC paste samples under bench-mounted Raman system and TG quantified CaCO<sub>3</sub>.**

	Wavenumber	Height	Area	Total CaCO <sub>3</sub> by TG (%)
0-2 mm	1084.4	10055.1	157497.8	25.2
5-7 mm	1085.0	9741.7	163658.3	21.4
10-12 mm	1085.0	3014.8	45534.2	8.7
15-17 mm	0	0	0	5.5
20-22 mm	0	0	0	5.1

**Table 7 Signal, noise and SNR values from optical fibre Raman and bench-mounted Raman systems.**

	Signal	Noise	SNR
Optical fibre Raman system	707.4	76.3	9.3
Bench-mounted Raman system	10055.1	124.2	81.0